ADVANCES IN GEOMATICS

VOLUME 04 • ISSUE 01 • APRIL 2026
e-ISSN: 3023-4980

ORIGINAL ARTICLE

Submission: 27/02/2026
Accepted: 18/04/2026

A BAYESIAN APPROACH TO INTEGRATE AND PREDICT LAND COVER CHANGES IN THE CONTEXT OF LAND SURFACE TEMPERATURE VARIATIONS USING MULTISPECTRAL REMOTE SENSING DATA

Nadeeka A.M.T.[1]* **Duminda WELIKANNA[2]**

[1] The State Key Laboratory of Information Engineering in Surveying, Mapping and Remote Sensing, Wuhan University, China .

[2] Department of Surveying and Geodesy, Faculty of Geomatics, Sabaragamuwa University of Sri Lanka, Sri Lanka.

* Corresponding Author: Nadeeka A.M.T., tharukaggc@gmail.com 0009-0004-4712-5553

ABSTRACT

Land Surface Temperature (LST) is an important geophysical parameter in global energy balance studies and hydrologic modeling. Many studies have suggested that there is a strong correlation between LST and Land Cover (LC) changes due to its sensitivity to vegetation cover. Due to rapid urbanization and population growth, significant changes in LC are caused, which directly contribute to climate change through a variety of processes causing changes in LST. Thermal remote sensing is sensitive to an object's temperature and emittance depending on the wavelength. The objective of this experiment is to build a mathematical model to investigate the relationship between LST and the LC changes in Sri Lanka. The model built in the study could be used to analyze relationships between parameters depending on their frequency distributions, which is quite useful in the applied science domain. The model is based on Bayes' theorem, which determines the conditional probability of the events. Landsat 8 OLI/TIRS images throughout 2015 to 2020 were classified into five LC classes as water, soil, vegetation, impervious, and cloud using Support Vector Machine (SVM) classification. LST was retrieved for the same period using the standard equations for LST retrieval by Landsat 8 using the normalized difference vegetation index (NDVI). Multispectral bands were used for the LC classification, and thermal bands were used to obtain the LST. Vegetation cover has been significantly affected by the changes in LST, while other LC types show a less significant relationship with the LST. The novelty of this study lies in applying a Bayesian probabilistic framework to quantify the degree of association between LC types and LST using frequency distributions. Unlike traditional correlation-based approaches, this model enables a more robust conditional probability estimation, offering a more nuanced understanding of how each LC type interacts with LST variations. This probabilistic insight can be particularly useful for predictive land management and climate modeling.

Keywords: Land Surface Temperature, Land Cover, Bayesian Theorem, Landsat 8, Support Vector Machine.

Cited As: Nadeeka, A. M. T., & Welikanna, D. (2026). A Bayesian Approach to Integrate and Predict Land Cover Changes in the Context of Land Surface Temperature Variations Using Multispectral Remote Sensing Data, Advances in Geomatics, 4(1), 1-34. https://doi.org/10.5281/zenodo.20541417

INTRODUCTION

Land surface temperature (LST) serves as a manifestation of the energy flow in the interactions linking the land surface with both atmosphere and biosphere (Tan et al., 2020) which is an important geophysical parameter in many aspects of the Geosciences mainly to get an overall understanding of land-surface processes at different scales. The temperature felt when the land surface is touched with the hands or the skin temperature of the ground is defined as the LST (Avdan & Jovanovska, 2016). Climate change and global warming have become two of the major concerns in recent decades. Global climate change, hydrological and agricultural processes, urban land use/land cover, Land and atmospheric effects, Crop management, water management, forest fire monitoring, urban heat islands, deforestation, draughts, surface water evapotranspiration are some of the applications of studying and measuring LST variations. Due to rapid urbanization and population growth significant changes in Land Cover (LC) are caused. Human activities are hugely affected by the Earth's vegetative cover which directly contributes to climate change through a variety of processes causing changes in LST. Many studies have suggested that there is a high correlation of LST the LC changes due to its sensitivity to vegetation cover and soil moisture.

Thermal remote sensing is sensitive to objects' temperature and emittance depending on the wavelength. Further, it also provides regional and global coverage at good temporal and spatial resolutions. Land surface temperature has a strong correlation with LC Changes and it could be estimated with a mathematical model developed using Bayes theorem. LST and LC are inherently related spatial parameters that could be assessed using Thermal and multispectral remote sensing respectively. LST varies spatially according to soil type, LC, and land use and temporally with the time of day and season of the year. Satellite observations are important for observing LST due to their spatial and temporal coverage (Richards & Jia, 2005, p. 195). Due to LC changes, rapid urban expansions are caused, which is highly affecting the ecological environmental process at local and regional levels (Guha et al., 2020).

Sun. Q. et al. have integrated remote sensing, GIS, landscape ecology, and statistical analysis methods to study the urban thermal environment in Guangzhou, China. They have focused on the different indices (NDVI, NDBI, NDBaI, and MNDWI) to analyze the relationships between land surface temperature (LST) and land use land cover (LULC) using multiple regression analysis with the Landsat 7 TM data. The elevation data extracted from the DEM has been added to the computation. The maximum likelihood classification method has been used for the LC classification. Finally, the study has revealed that LST increased with the density of urban built-up and barren land due to sparse vegetation and bare soil in barren lands. LST has decreased with vegetation cover (forest, grassland, and cropland), where forest had the highest mean NDVI. Water has the lowest mean NDVI but not the highest mean LST, which is due to the high thermal inertia and convection of water. The correlation between MNDWI, DEM, and LST was found to be negative, which implies that pure water would

decrease the surface temperature and polluted water would increase the surface temperature. Both the qualitative and quantitative analysis of this study showed that land use has a great influence on LST. Therefore, the results obtained by the study could be used to mitigate the urban heat island effect with appropriate land use planning.

Sandipta Das, S., and Angadi, D.P., have used Landsat TM/ETM+ data seasonally (January, April, and November) to identify LST variations for two different periods of 1990 and 2016 in their case study of Barrackpore Subdivision, West Bengal, India. Different indices; the normalized difference vegetation index (NDVI), the normalized difference moisture index (NDMI), the normalized difference built-up index (NDBI), and the normalized difference water index (NDWI) were derived, and regression analysis was used to analyze and validate the relationship between LST and LULC. The spatial autocorrelation method of the Getis-Ord Gi formula has been used to delineate the concentration of hotspot and cold spot areas. The positive correlation between LST and NDBI has confirmed that impervious surfaces have strongly influenced the increase in surface temperature. They could have revealed that vegetation, water bodies, and wetlands are negatively related to LST while built-up land is positively related. The positive correlation exhibited by the Seasons statistical relationship between LST and NDBI has confirmed that impervious surfaces have strongly affected surface temperature. The regression line has shown a negative relationship between LST and wetlands and waterbodies, which shows the LST effects are very low over extremely humid or moist areas. They have considered only two years for the analysis. The obtained results may be stronger if they could consider some more years between the considered 25 years. The study could be used by the municipal authority to implement new decision policies and management to reduce the effects of LST on sustainable development in the future

A time series analysis was carried out as a case study in the Atlanta metropolitan area by Fu. P. and Weng. Q. to illustrate LULC change and its impact on land surface temperature (LST) variations using the Landsat TM/ETM+ images from 1984 to 2011. The LCs were classified as water, barren land, shrub land, urban-low intensity, urban medium intensity, urban-high intensity, crops, herbaceous, pasture, and woody wetlands using the Continuous Change Detection and Classification (CCDC) algorithm. The classification accuracy was checked with the Random Forest. The time series LSTs were determined using the single channel algorithm, which can derive LSTs independent of most of the necessary atmospheric profiles in empirical ways with high accuracy. This algorithm required only the parameters of water vapor and land surface emissivity. The final results were performed with an average classification accuracy of 89% and a change detection accuracy of 92%. The cloud-, cloud shadow and snow-contaminated pixels are excluded from the analysis. The larger trend change of the urban LCs has shown the LSTs were influenced by the urbanization-induced LC changes. They have identified that the conversion of evergreen forests to medium-intensity urban land generated the largest difference in annual LST variation. To reduce the outlier effects, the study has used the locally

weighted regression smoother (LOESS) scheme for the decomposition analysis. The effectiveness of the algorithm may depend on the number of clear-sky pixels available for the study area.

Guha, S., et al. have focused on estimating the land surface temperature of Raipur City in India, emphasizing the urban heat island (UHI) and non-UHI inside the city boundary and their relationship with LULC using Landsat 8 (OLI/TIRS) data. NDVI, NDWI, and NDBI were used to perform LULC classification for vegetation, water, and built-up areas, respectively, and the NMDI index for dry soil and bare lands. The study has been carried out on four satellite images, considering four different seasons: pre-monsoon, monsoon, post-monsoon, and winter in the same year. The mono-window algorithm was used to derive LST, where ground emissivity, atmospheric transmittance, and effective mean atmospheric temperature are considered the three required parameters. MODIS datasets have been used for the validation of LST values as a reference image instead of taking in situ field measurements. They could identify the strongest correlation between LST and the LULC indices during the monsoon and post-monsoon seasons, while winter and pre-monsoon images show a comparatively weak correlation. In this study, the relationship between LST and some weather and terrain components has been analyzed, including elevation, wind speed, humidity, air temperature, and air pressure. A strong positive relationship was identified between air temperature and LST, while LST and air pressure had a strong negative relationship. LST and wind speed correlate moderately negatively, and humidity and LST have a weakly negative relationship. No linear correlation was found with the elevation. A negative relationship was observed between NDVI and NMDI with LST, while a positive relationship was observed with NDBI. No significant relationship has been identified between LST and NDWI. Furthermore, the relationships of LST to NDVI, NDWI, NDBI, and NMDI have been interpreted quantitatively by linear regression analysis (using Pearson's product-moment correlation coefficient) at the pixel level. This study can be further developed by considering other LULC indices such as the enhanced vegetation index, soil adjusted vegetation index, modified normalized difference water index, normalized difference mud index, burn area index, etc. to examine the better correlation with LST and other statistical methods and algorithms like the Spearman Rank Correlation Coefficient, the Kendall Correlation Coefficient, etc. to estimate the correlation between LST and different LULC indices.

Tan. J. et al. have studied the Dongting Lake area (China), which is a climate change-sensitive and ecologically fragile area, to determine the relationship between LST and LULC using Landsat TM/ETM+, DEM, and MODIS data. A single-window algorithm was used for the LST retrieval, which had the greatest consistency with the actual measurements. Also, the results were compared with the MODIS temperature products from the same time and identified a relative error of 2% or less. Using the decision tree methodology, which is based on the classification and regression tree (CART) algorithm for the LULC classification, the area was categorized into nine categories: water bodies, riparian forest, marshland, paddy fields, reed beach land, mud beach land, dry land, built-up land, and forest

land. The results showed that LST is significantly affected by LULC types. The LST of forest land and dryland is higher than that of other land types, and the LST of water bodies is much lower than that of other land types and also much lower than the mean LST of the study area. The NDMI showed a strong negative spatial correlation with LST, while the DEM, NDVI, and distance showed a weak spatial correlation with LST. This exploration of regional LULC and climate change patterns and processes can provide a typical case for a larger range of global change studies

Rheea.J. et al. have investigated the relationship between LC patterns and surface temperature using an advanced machine learning technique (random forest as well as simple linear regression). The purpose was to derive important spatial metrics of LC affecting surface temperature to provide information for alleviating heat stress and reducing the adverse impacts of drought in urban areas, considering two urban sites in Denver, Colorado, USA. Random forest is based on an ensemble approach to predicting a target variable by combining predictions from multiple Classification and Regression Trees (CART), which has the robustness to counteract noise, outliers, and overfitting. The LC map was derived from light detection and ranging (LiDAR) data with 0.5 m spatial resolution, and the LST map was derived using Landsat 5 Thematic Mapper (TM) data with 120 m spatial resolution. Maps were classified into four LC types: buildings, trees, grass, roads, and parking lots. Only trees, roads, and parking lots showed significant spatial metrics affecting surface temperature using both methods in their study. The results of this study provide information that can be used for planting trees and locating parking lots to alleviate heat stress in urban areas, especially during the summer. These measures can be used to reduce the adverse impacts of urban drought since the heat wave and drought are closely related and affect each other. The effect of land use on surrounding regions was not considered for analyses such as those of nearby large waterbodies, which affect large-scale circulations of climate and meteorological events

Many studies have suggested that there is a strong correlation between LST and LC changes due to their sensitivity to vegetation cover. The relationship between these two parameters has been scrutinized using regression-based analysis, mainly linear regression, in previous studies. However a model to integrate these parameters into a single framework is not being investigated or developed. The problem is to be addressed using a contextual Bayesian approach in the study. In regression analysis, the best-fitting value is determined by considering all the available data without considering the precision of the values, where outliers are also considered. The proposed Bayesian method directly gives the actual probability according to the occurrence of the events. It calculates the exact conditional probability of each single event within the 3*3 moving window, which is not affected by all the values in the dataset.

This experiment was performed to investigate the relationship between LST and LC using a mathematical model based on Bayes Theorem. Time series analysis was performed in this study from 2015-2020 to obtain LST and LC for each selected study area using the standard equations provided for

LST retrieval by Landsat 8 and SVM classification respectively. Here, five different cities with divergent climate conditions and three national forests were selected as the study area. Based on satellite images, vegetation Indices are used to estimate the percent vegetation cover in each pixel (Purevdorj et al., 2010) which is used for emissivity calculation in the LST retrieval process. The model built in the study could be used to analyze the relationship between parameters depending on their frequency distributions, which is quite useful in the applied science domain.

DATA AND METHOD

Model development

The model is developed based on two sample datasets (8 by 8 matrices) of LST and LC values, including five LC classes and five LST values.

29	29	29	28	28	27	27	28
29	29	28	28	27	27	27	27
29	28	28	26	27	27	27	28
28	28	28	28	29	29	28	28
28	28	28	27	27	27	28	28
29	26	28	28	27	27	27	28
28	28	28	28	29	29	28	28
28	28	28	27	27	27	28	26

(a)

1	1	1	2	2	3	3	3
1	1	2	2	2	3	3	3
1	2	2	4	3	1	3	2
2	2	2	1	1	1	2	2
2	2	3	3	3	2	1	2
1	4	3	2	1	1	2	2
2	2	2	2	1	1	2	2
2	2	2	3	3	3	2	4

(b)

Figure 1. (a) sample dataset for LST with values 26,27,28,29; (b) sample dataset for LC with values 1,2,3,4. Highlighted pixels show the respective LC classes when the LST value is 27.

A 3 by 3 moving window is considered to check the direct influences of neighboring pixels for probability calculation in each center pixel, and the resultant probability images are used for the analysis. The model development coding was done with MATLAB programming language.

27	27	28
27	27	27
29	29	28

3	2	1
1	1	2
1	1	2

P (1) = (5/9)
P (27|1) = (2/5)
P (27) = (5/9)

Figure 2. Probability calculation for the center pixel being LC class 1 for given LST value 27.

P (1|27) = P (1) *P(27|1)/P (27)

= (5/9) *(2/5)/ (5/9)

= (2/5)

Resulting probability - Conditional Probability of LC with respect to LST

The model was developed using equation (1), which calculates the conditional probability of each LC class concerning each LST value.

$$P_{t1}(\omega \mid T) = \frac{P_{t1}(\omega \cap T)}{P_{t1}(T)} = \frac{P_{t1}(\omega) * P_{t1}(T \mid \omega)}{\sum^{pixels(t_1)} P_{t1}(T) * P_{t1}(T \mid \omega)} \quad (1)$$

There are four unique LST values and four unique LC values included in the sample dataset. Therefore, four probability images per one LST class were generated by the model (for example: for LST value 26, the created probability images are related to the P (1|26), P(2|26), P(3|26), and P(4|26)). The same procedure was followed for each LST value, and finally, 16 probability images (4*4) were created. The highly affected LC for each LST value can be determined by the images with the highest probability; therefore, the highest probability images were selected by image plot analysis, and the percentage for the highest probability was calculated. Then the LC with the highest percentage was assigned to each LST value. See Appendix A for all probability images generated by the model for each area.

Table 1. Percentage for each LC in the highest portability images.

LST	LC	Percentage
26	4	100
27	3	62.5
28	2	81.5789
29	1	100

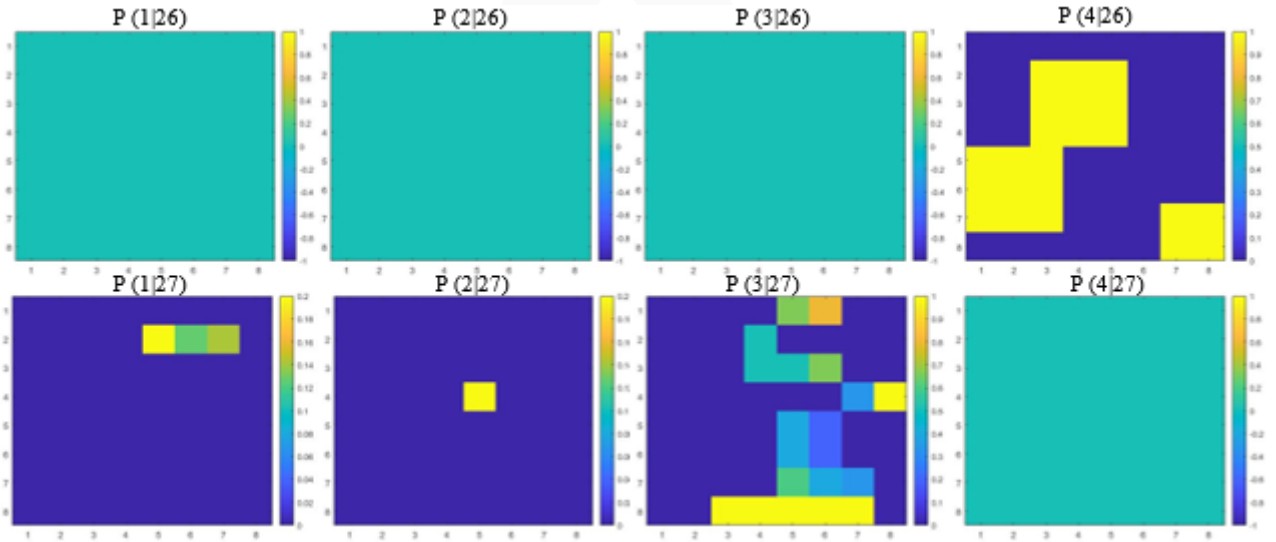

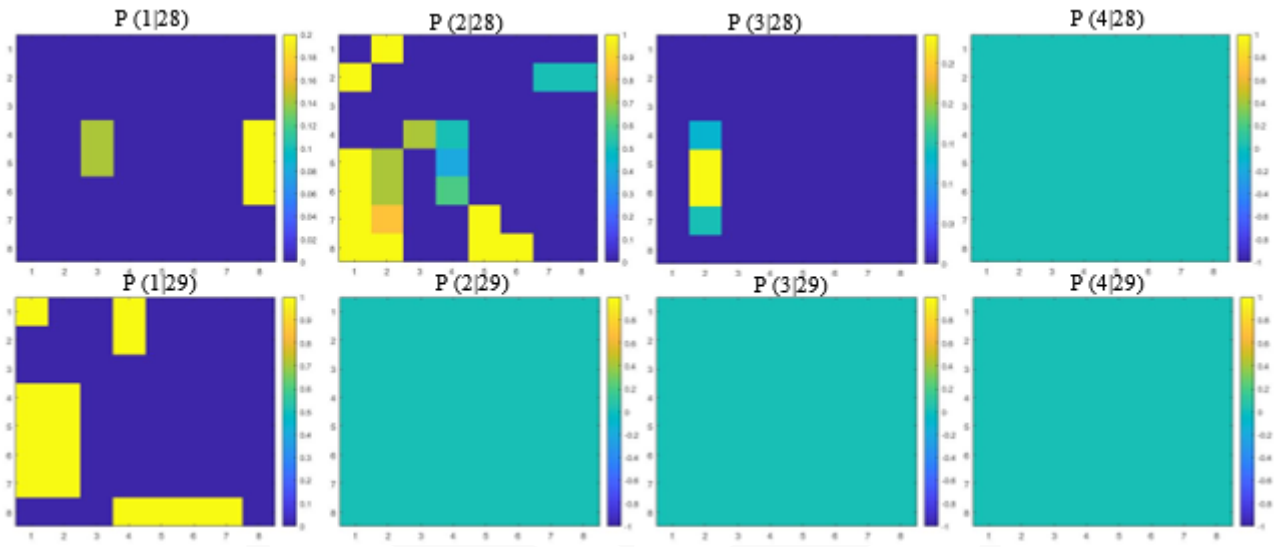

Figure 3. Highest probability for LST 26 with LC 4, LST 27 with LC 3, LST 28 with LC 2, and LST 29 with LC 1.

P(4|26)

0	0	0	0	0	0	0	0
0	0	1	1	1	0	0	0
0	0	1	1	1	0	0	0
0	0	1	1	1	0	0	0
1	1	1	0	0	0	0	0
1	1	1	0	0	0	0	0
1	1	1	0	0	0	1	1
0	0	0	0	0	0	1	1

P(3|27)

0	0	0	0	0.67	0.8	0	0
0	0	0	0.5	0	0	0	0
0	0	0	0.5	0.5	0.7	0	0
0	0	0	0	0	0	0.33	1
0	0	0	0	0.4	0.2	0	0
0	0	0	0	0.4	0.2	0	0
0	0	0	0	0.6	0.4	0.33	0
0	0	1	1	1	1	1	0

P(2|28)

0	1	0	0	0	0	0	0
1	0	0	0	0	0	0.5	0.5
0	0	0	0	0	0	0	0
0	0	0.71	0.5	0	0	0	0
1	0.71	0	0.4	0	0	0	0
1	0.71	0	0.6	0	0	0	0
1	0.86	0	0	1	0	0	0
1	1	0	0	1	1	0	0

P(1|29)

1	0	0	1	0	0	0	0
0	0	0	1	0	0	0	0
0	0	0	0	0	0	0	0
1	1	0	0	0	0	0	0
1	1	0	0	0	0	0	0
1	1	0	0	0	0	0	0
1	1	0	0	0	0	0	0
0	0	0	1	1	1	1	0

Figure 4. Highest probability Images for sample data sets which representing the best relationship of LC classes with each LST value; LST 26 with LC class 4, LST 27 with LC class 3, LST 28 with LC class 2 and LST 29 with LC class 1.

Model validation

The model validation is performed for a well-known area where the LC had a significant change in two consecutive years with Landsat OLI/TIRS Level-1 thermal and multispectral bands data by obtaining their LST and LC classification respectively. The LST estimation has done using the standard equations related with the NDVI and the Support vector machine (SVM) is used for the LC classification. Google earth and the Land Use LC maps are used as reference for LC classification.

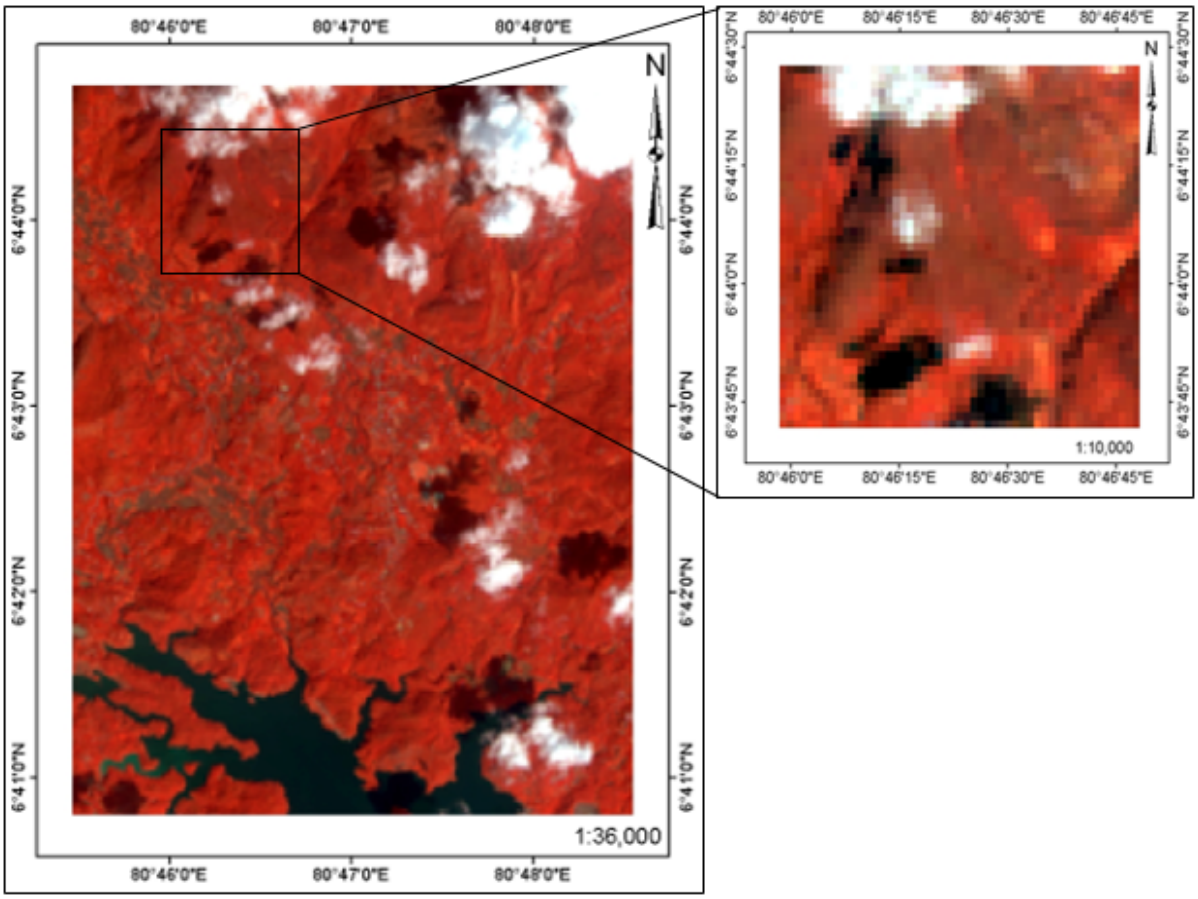

Figure 5. False color composite image in 2015, Belihuloya showing the area before the huge landslide occurred in 2016 with the zoom image; where the LCs were identified as vegetation and cloud.

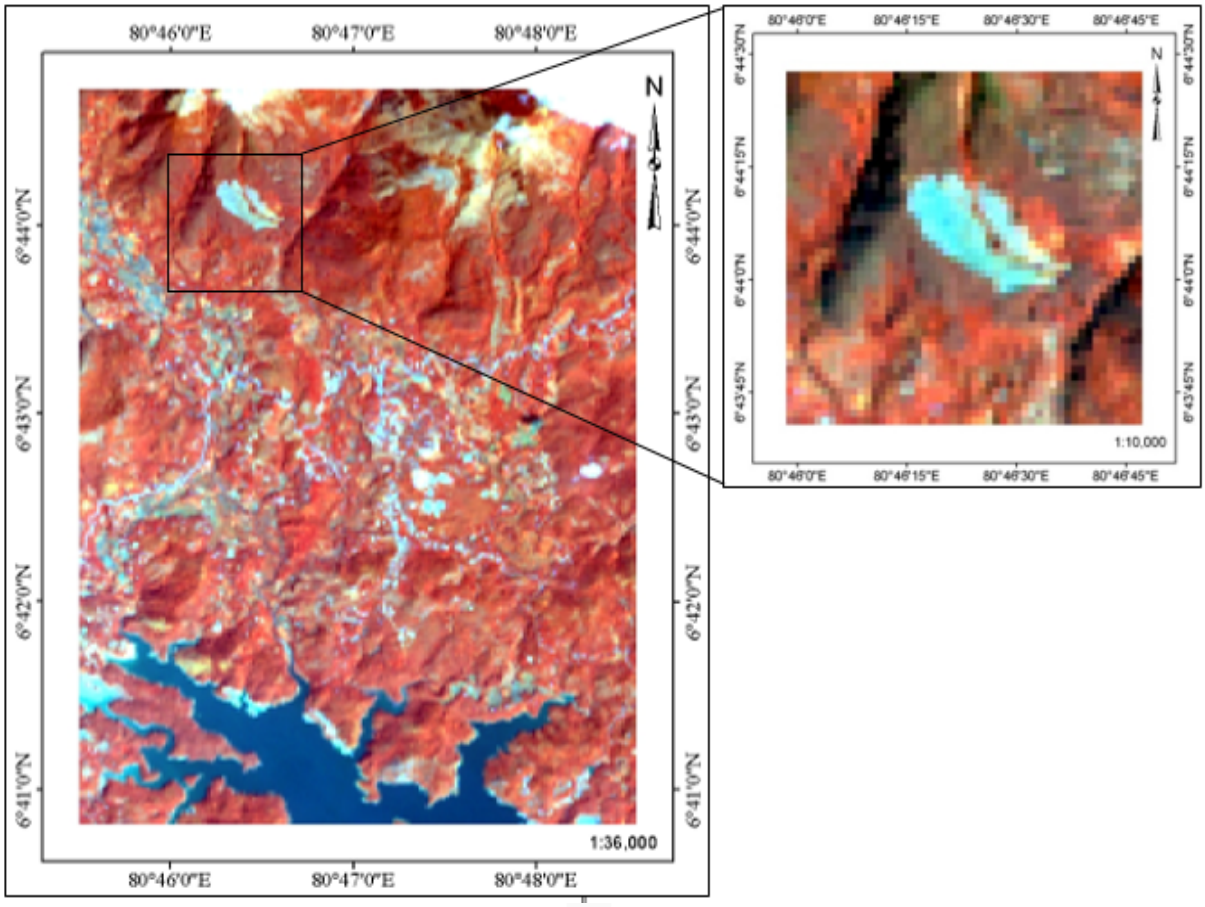

Figure 6. Comparison of LC change in Belihuloya, Sri Lanka area with Landsat 8 OLI\TIRS false-color composite images in 2016 where a huge landslide occurred and the vegetation cover has altered into Soil which is represented by the blue color patch of the zoomed image.

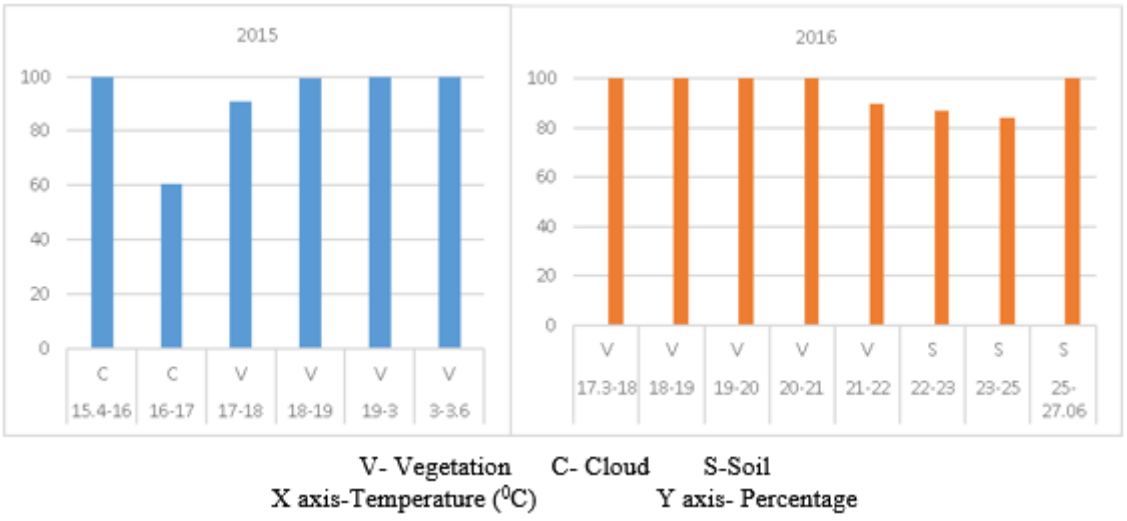

Figure 7. Model validation results that show Highly affected LCs percentage for LST ranges in 2015 and 2016 in the Belihuloya area with the changes of land covers in 2016 due to the landslide in this area.

The average LST for Belihuloya in 2015 was 18.76 C, and in 2016, it was 19.86 C. The highly affected LC classes were analyzed for each land surface temperature range. The model clearly shows that the LST increment has occurred due to the change of LC from vegetation to soil in 2016.

Regression analysis was performed with the R programming language and checked the relationship between the LST and LC classes for the selected area. It showed that the lowest LST values occurred due to the cloud cover, and the middle LST values were created by vegetation cover. The highest LST values occurred due to the soil cover in 2016. The regression analysis has also proved that the LC change has had a significant impact on the LST increment in 2016.

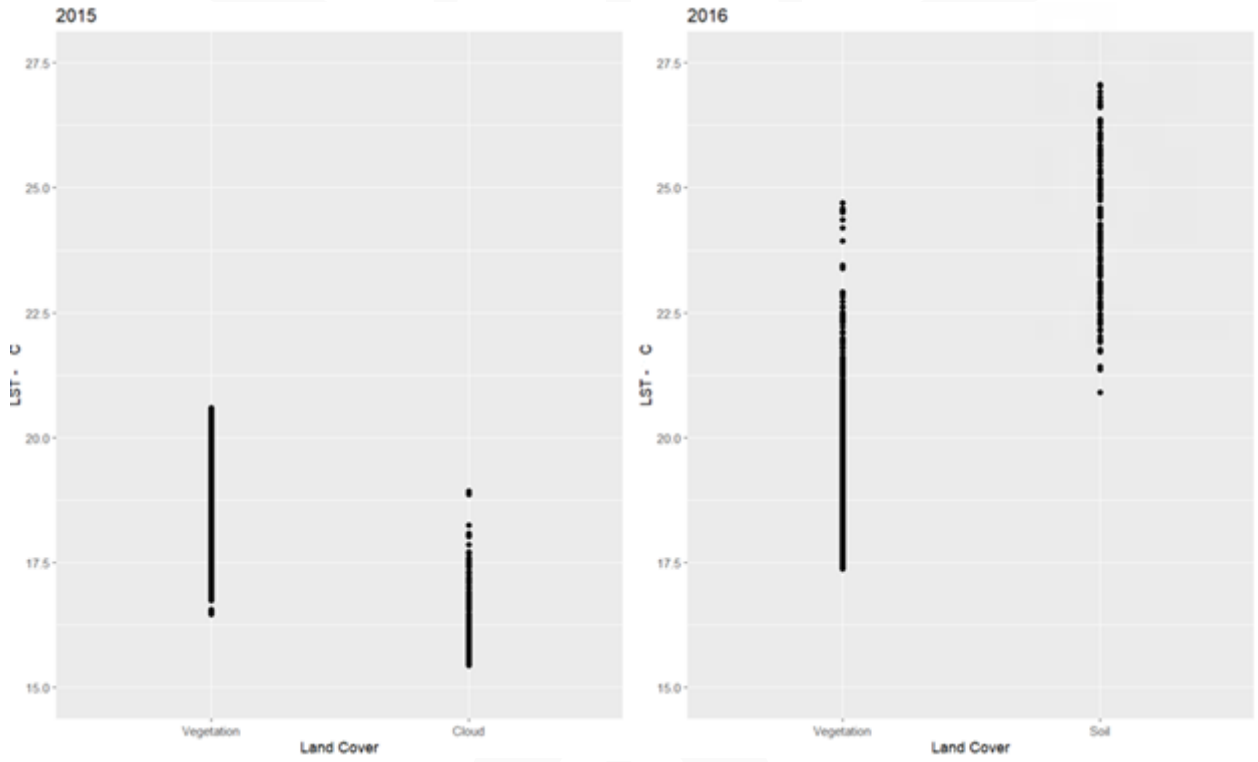

Figure 8. Regression Analysis for LST vs LC in 2015 and 2016 in Belihuloya area.

Land surface temperature calculation

Thermal band (Band 10, wavelength 10.60 µm –11.19 µm), Near Infrared band (band 5, wavelength 0.85 µm – 0.88 µm), and red band (band 4, wavelength 0.64 µm –0.67 µm) in Landsat 8 OLI/TIRS sensor data were used for LST calculation as shown in the following equations. The thermal band, Band 11, has not been used for the calculations due to its larger uncertainty in calibration with the recommendations of the USGS following January 6, 2014. This thermal band (band 10) was resampled using the nearest neighbor algorithm with a pixel size of 30 m to match the optical bands.

Top of atmospheric spectral radiance

$$L\lambda = ML * Qcal + AL - O_i \quad (2)$$

where ML represents the band-specific multiplicative rescaling factor (0.000342), Qcal is the Band 10 image, AL is the band-specific additive rescaling factor (0.1), and Oi is the correction for Band 10 (0.29) (Barsi et al., 2014).

Conversion of radiance to at-sensor temperature

$$BT = \frac{K2}{\ln[(K1/L\lambda)+1]} - 273.15 \quad (3)$$

where K1(1321.08) and K2 (777.89) stand for the band-specific thermal conversion constants from the metadata. For obtaining the results in Celsius, the radiant temperature is revised by adding the absolute zero (approx.–273.15 C) (Xu et al., 2004).

Calculating NDVI

Normalized Difference Vegetation Index (NDVI) can be used to calculate the Emissivity using percent vegetation of each pixel. For Landsat 8 OLI/TIRS images, Band 5 is representing NIR band and Band 4 is representing the red band. Following equation is used to calculate the NDVI

$$NDVI = \frac{NIR(Band5) - R(Band4)}{NIR(Band5) + R(Band4)} \quad (4)$$

NDVI was calculated in order to estimate land surface emissivity (LSE), which is a critical parameter for accurate LST retrieval. Since emissivity varies with vegetation density, NDVI provides a reliable way to determine the proportion of vegetation in each pixel. This step is therefore essential to correct for emissivity differences across land cover types and to improve the accuracy of the LST calculation

Calculating the proportion of vegetation

$$P_V = \left(\frac{NDVI - NDVI_{Min}}{NDVI_{Max} - NDVI_{Min}}\right)^2 \quad (5)$$

Calculating land surface emissivity (LSE)

$$\varepsilon = 0.004 * P_V + 0.986 \quad (6)$$

LSE is the efficiency of transmitting thermal energy across the surface into the atmosphere which is a proportionality factor that scales blackbody radiance (Planck's law) to predict emitted radiance. (Sobrino et al., 2004; Qin et al., 2001)

The constants 0.004 and 0.986 in the LSE equation are derived from empirical studies (e.g., Sobrino et al., 2004; Qin et al., 2001) that established a linear relationship between vegetation proportion (PV) and emissivity. These values have been widely used in LST retrieval studies using Landsat data

and are recommended in the remote sensing literature. They were chosen to ensure methodological consistency with previous research and to allow comparability of our results with other studies.

Retrieving the LST

$$Ts = \left(\frac{BT}{1 + [(\lambda BT / \rho) \ln \varepsilon \lambda]} \right) \quad (7)$$

where Ts is the LST in Celsius (C, (2)), BT is at-sensor BT(C), λ is the wavelength of emitted radiance (for which the peak response and the average of the limiting wavelength (λ=10.895) (Markham et al., 1985).

$$\rho = h\frac{c}{\sigma} = 0.01438mK \quad (8)$$

where σ is the Boltzmann constant (1.38 x 10^{-23} J/K), h is Planck's constant (6.626 x 10-^{34} J s), and c is the velocity of light (2.998 x 108 m/s) (Weng et al., 2004).

Using the above equations LST maps were generated and LST classes were assigned according to the color density of the generated map using density slice analysis. Finally obtained LST classes were transformed into .txt format and used as the LST input for the model. See appendix B for the LST Class maps of each area in each year.

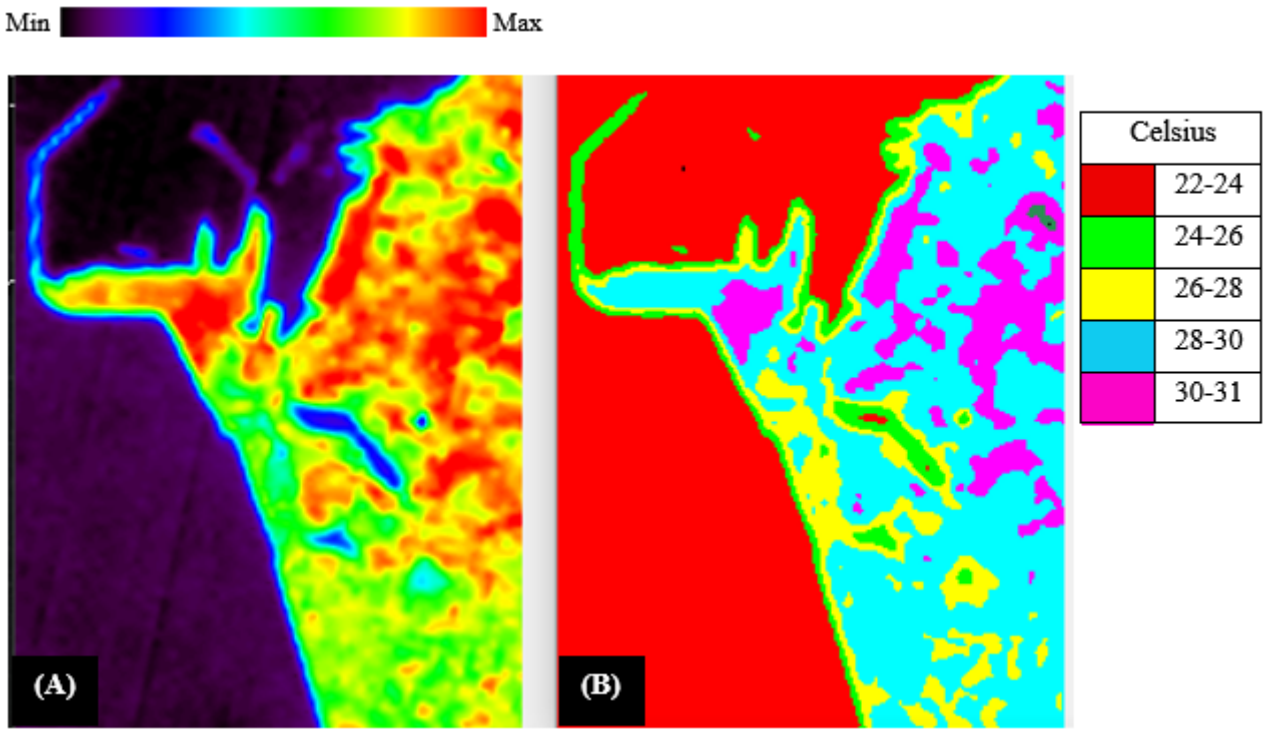

Figure 9. LST map (A) Generated for Colombo Area in 2016 and the LST class map (B) for the same area.

Land cover classification

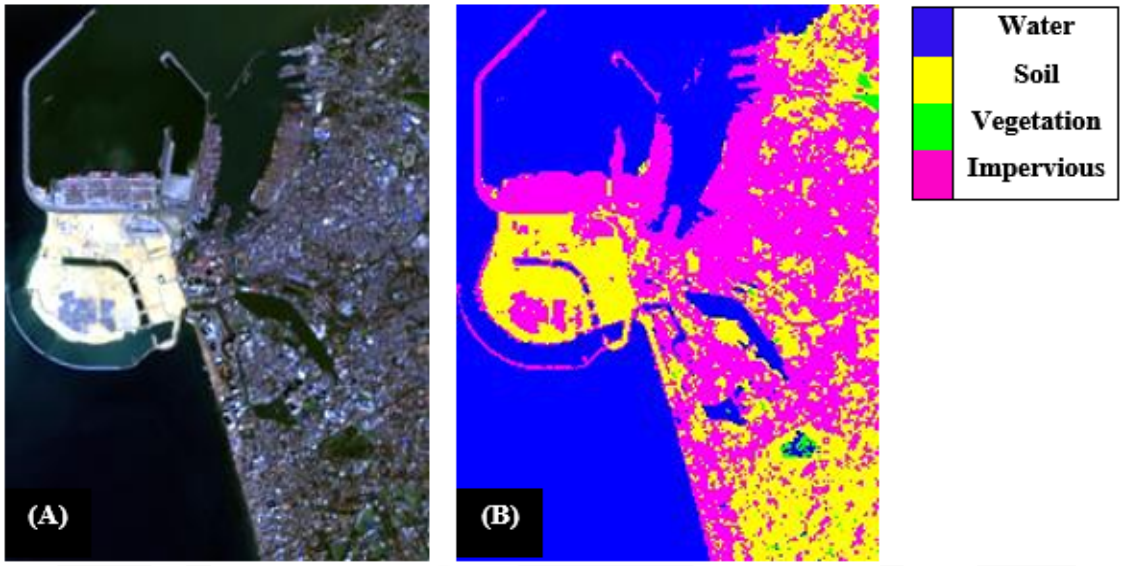

Figure 10. True color composite image(A) for Colombo Area in 2018 and the LC classification map (B) of the same image using SVM Classification showing the completed port city area.

Five major LCs were considered in the study as Vegetation, Water Impervious, Soil and Cloud. LC classification was performed with the Support Vector Machine Classification for each selected area. Google earth maps and Land Use LC maps by the Survey Department Sri Lanka were used as the reference data for sample generating.

Following the above procedure, the processing of LST retrieval and LC classification was done for the selected five cities from 2015 to 2020.These images were the input for the developed model in text format. As the output of the model, conditional probability of each LC class with respect to each LST values in each pixel of the image were calculated and after analyzing the obtained probability mages highly affected LC classes for each LST class was identified.

RESULTS

Colombo is the commercial capital and the largest city in Sri Lanka by population, which makes it a highly urban area. The LC maps are clearly showing how the LCs are changed in Colombo from 2015. The major change has occurred due to the construction of the port city, which spans 269 hectares of reclaimed land from the sea. Due to the absence of vegetation cover, the area is showing a higher LST compared with the other areas in the study, which have an average of 25.52 C. The model shows the lowest LST values are due to the water surface, and the highest are due to the impervious surface. The regression analysis shows that both the impervious and soil classes are highly affected by the higher LST values, and the Bayesian model has proven that impervious surfaces have had the greatest effect on the highest LST in each year except for 2020.

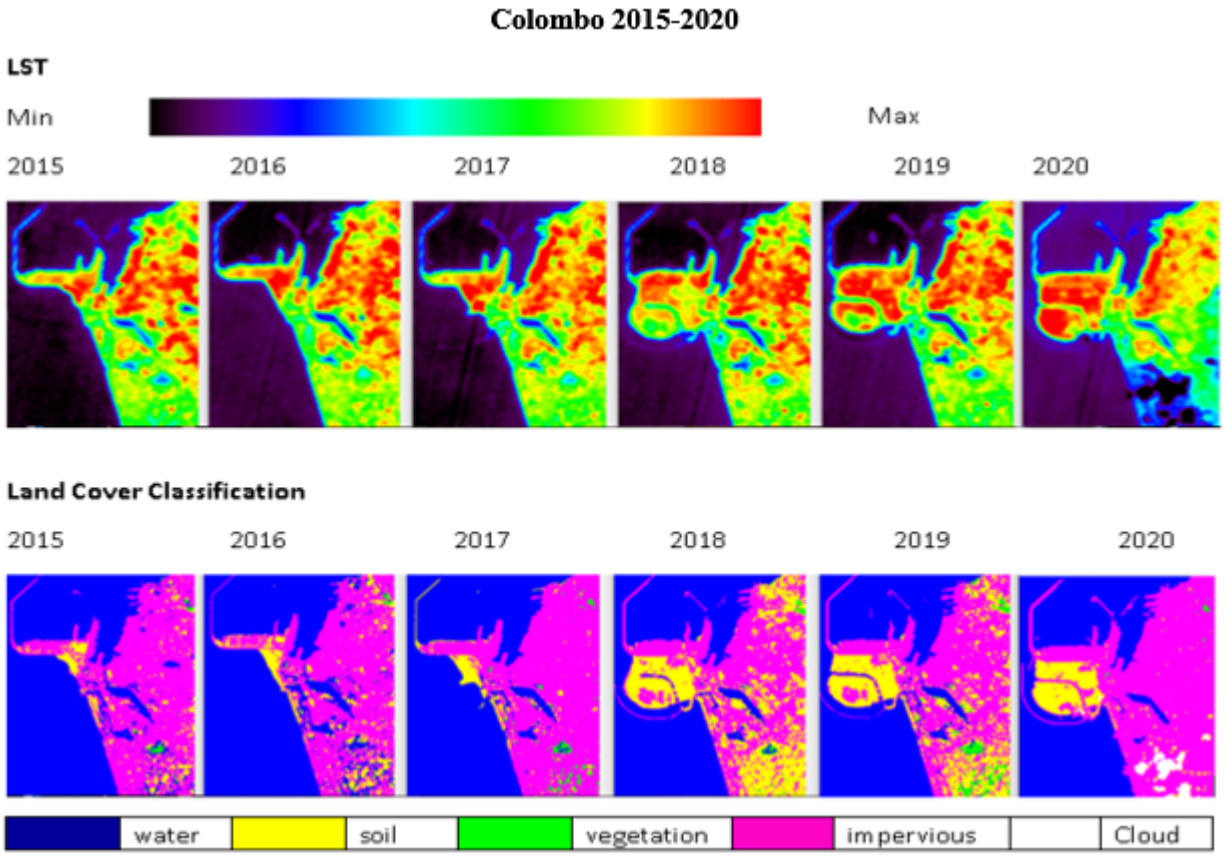

Highly effected LC classes for each LST range for Colombo area from 2015 to 2020

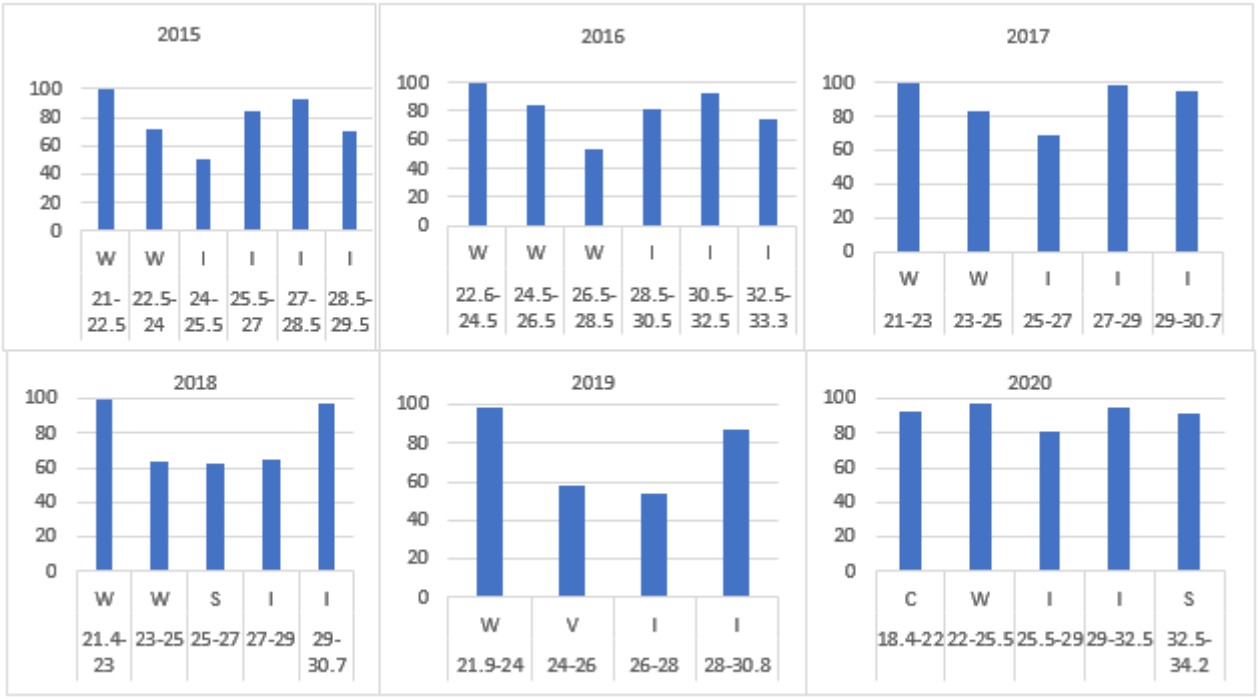

W-water I-Impervious V- Vegetation C- Cloud S-Soil

X axis-Temperature(^{0}C) Y axis- Percentage

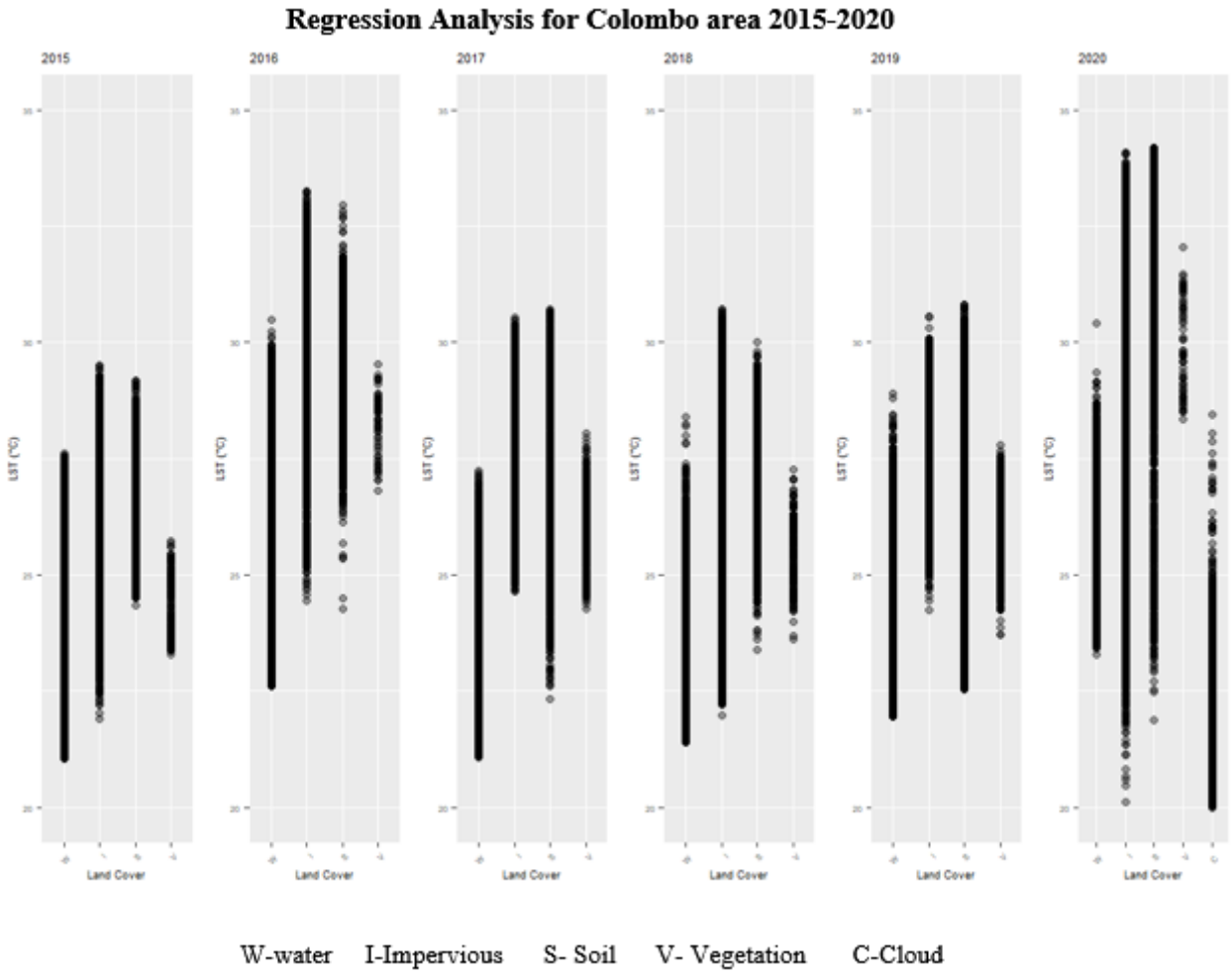

Figure 11. LST map, LC map, highly affected LCs and regression analysis of Colombo area from 2015-2020.

Ratnapura is very famous for being the gem trading center of Sri Lanka, which has a tropical rainforest climate. The study area consisted of a part of the 'Kalu River', which is the main irrigation source in the area. The area contains around 68% vegetation and 29% impervious surface. The model has shown that the impervious surface has contributed to the highest LST in the town area, and cloud cover and vegetation have affected the lower values of LST. The average LST has been recorded at 24.20 C throughout the 6 years, and the highest LST has been recorded in 2019 at 26.02 C while the minimum has been recorded in 2015 at 22.95 C. The regression analysis shows that the soil and impervious surfaces are highly affected for the highest LSTs in the area, while the clouds and vegetation are affected for the lowest LST.

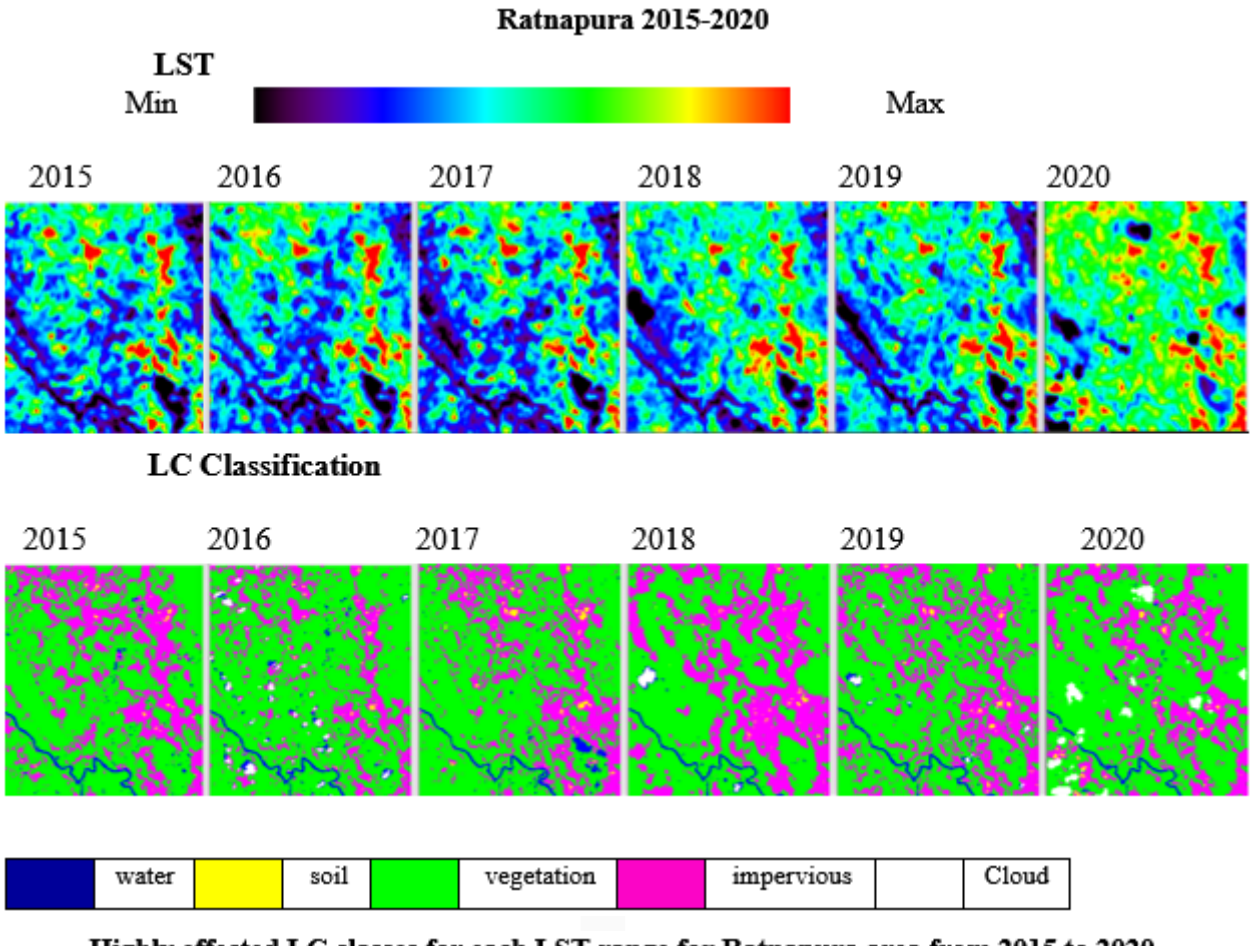

Highly effected LC classes for each LST range for Ratnapura area from 2015 to 2020

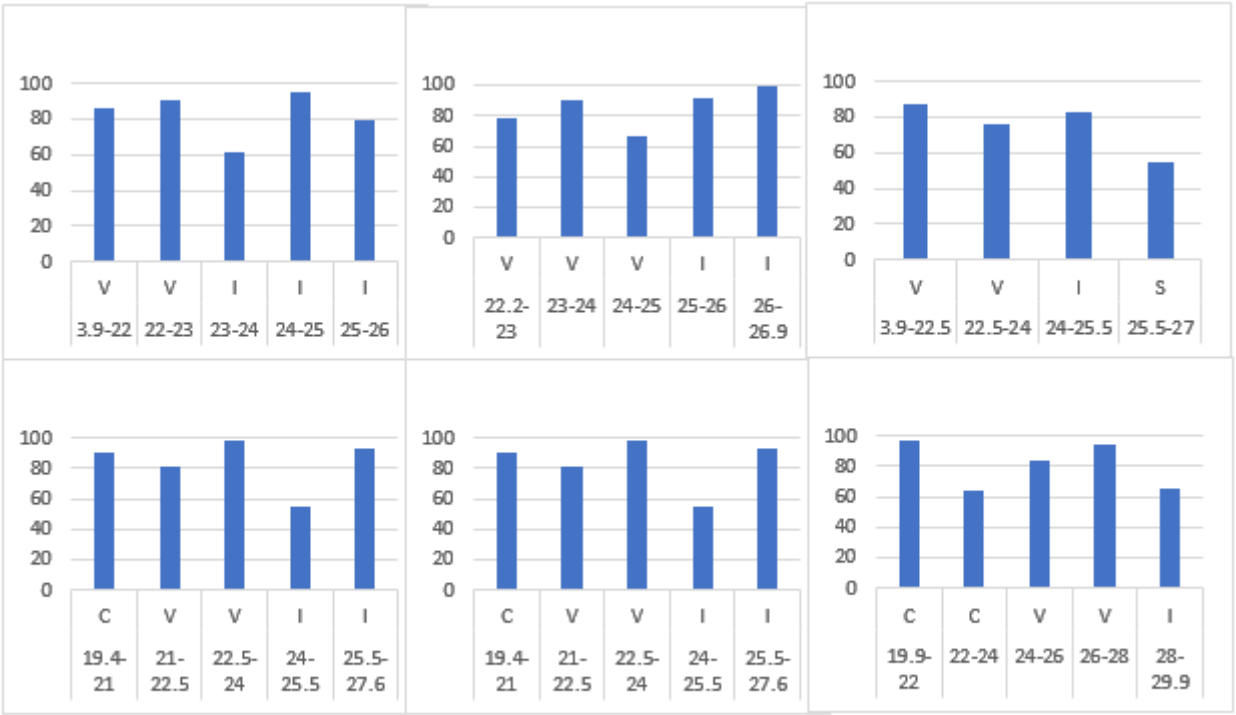

W-water I-Impervious V- Vegetation C- Cloud S-Soil

X Axis-Temperature(^{0}C) Y axis- Percentage

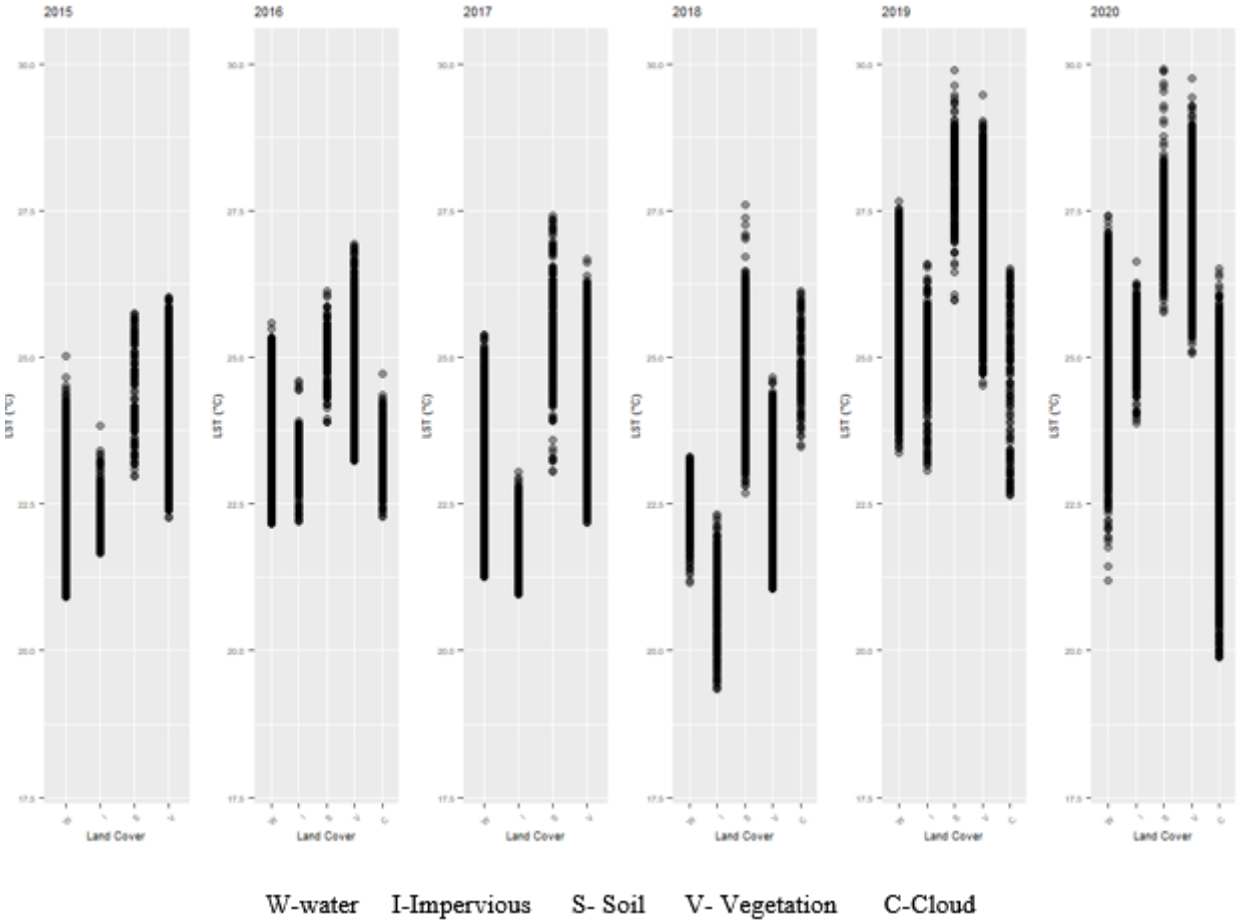

Figure 12. LST map, LC map, highly affected LCs and regression analysis of Ratnapura area from 2015-2020.

Kandy is a major tourist destination with a cooler climate than the coastal regions of Sri Lanka. The LC maps show the area contains a highly vegetated area of around 54% and an impervious surface of around 22%. The average LST has recorded as 24.67 C where the minimum and maximum LST has recorded as 22.4276 C and 28.53 C. The model has shown that the higher LST values are caused by the impervious surface, while the lower LST values are highly affected by the vegetation cover. According to the regression analysis, water and soil have contributed to the middle LST values, and impervious has contributed to the highest LST values in each year. The trend analysis of this Kandy area shows the LST has a great positive correlation with the impervious surface and a negative correlation with the vegetation.

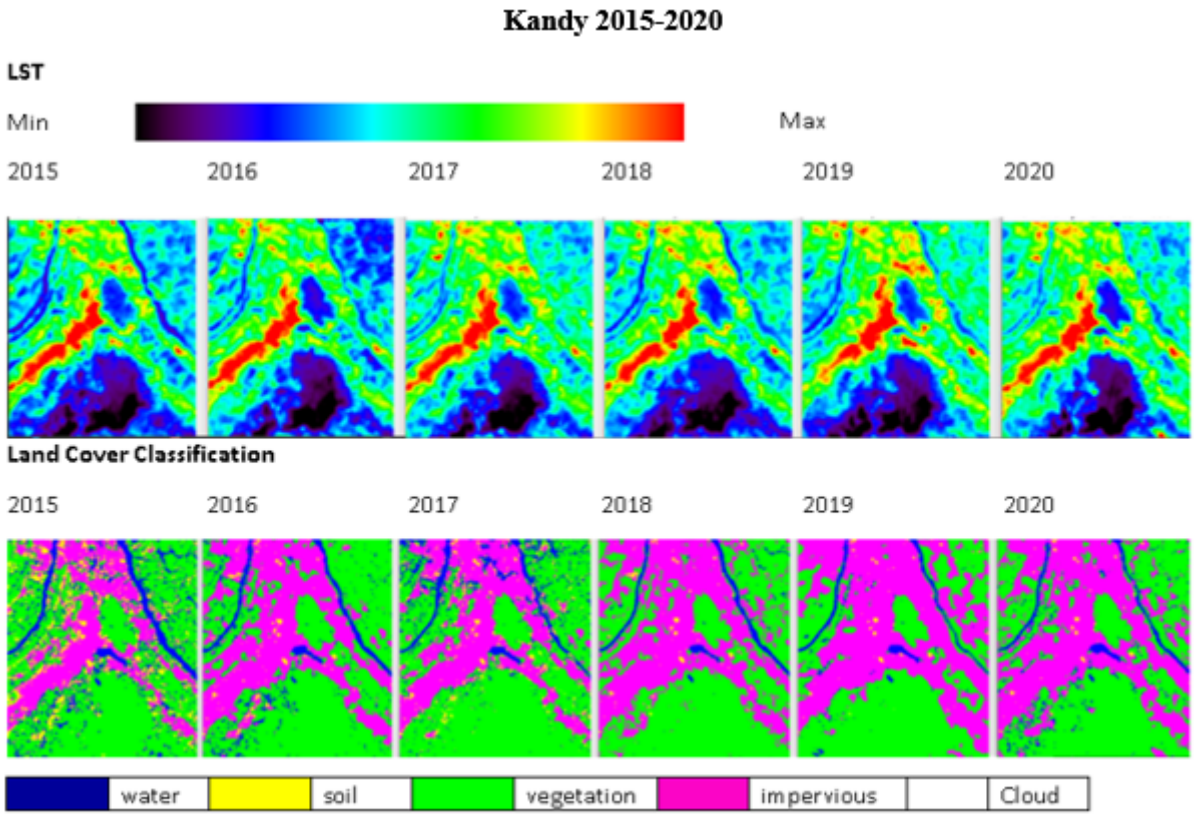

Highly effected LC classes for each LST range for Kandy area from 2015 to 2020

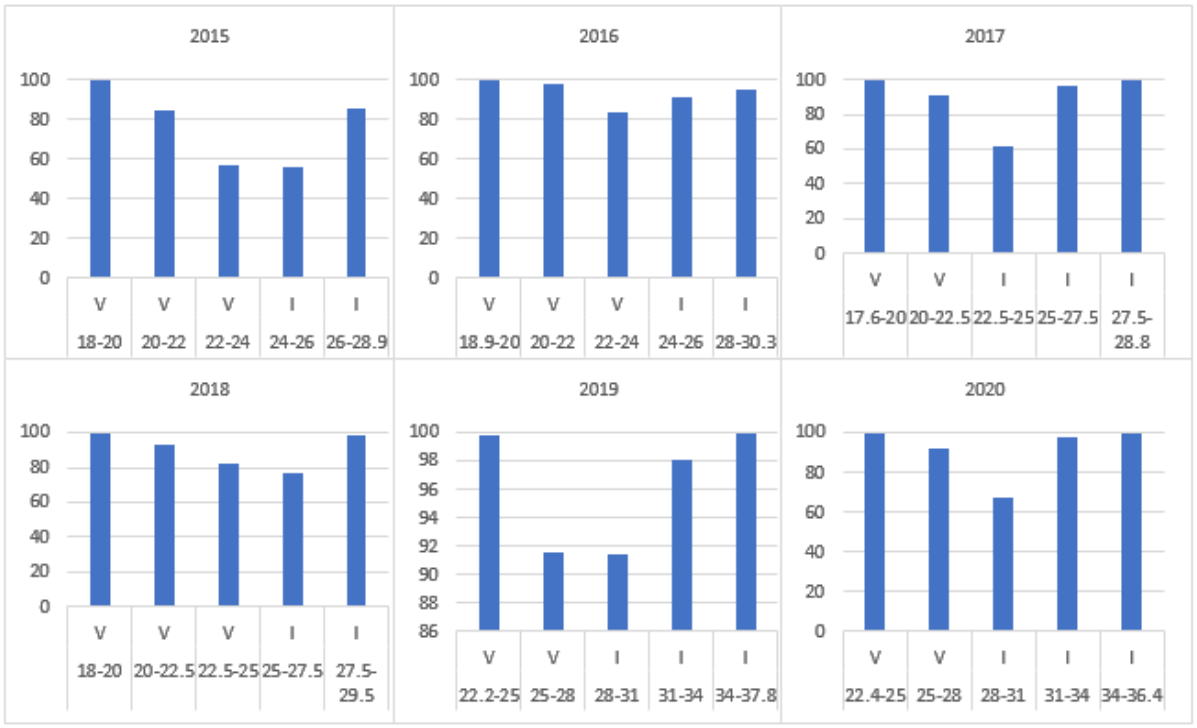

W-water I-Impervious V- Vegetation C- Cloud S-Soil

X – axis -Temperature(^{0}C) Y - axis- Percentage

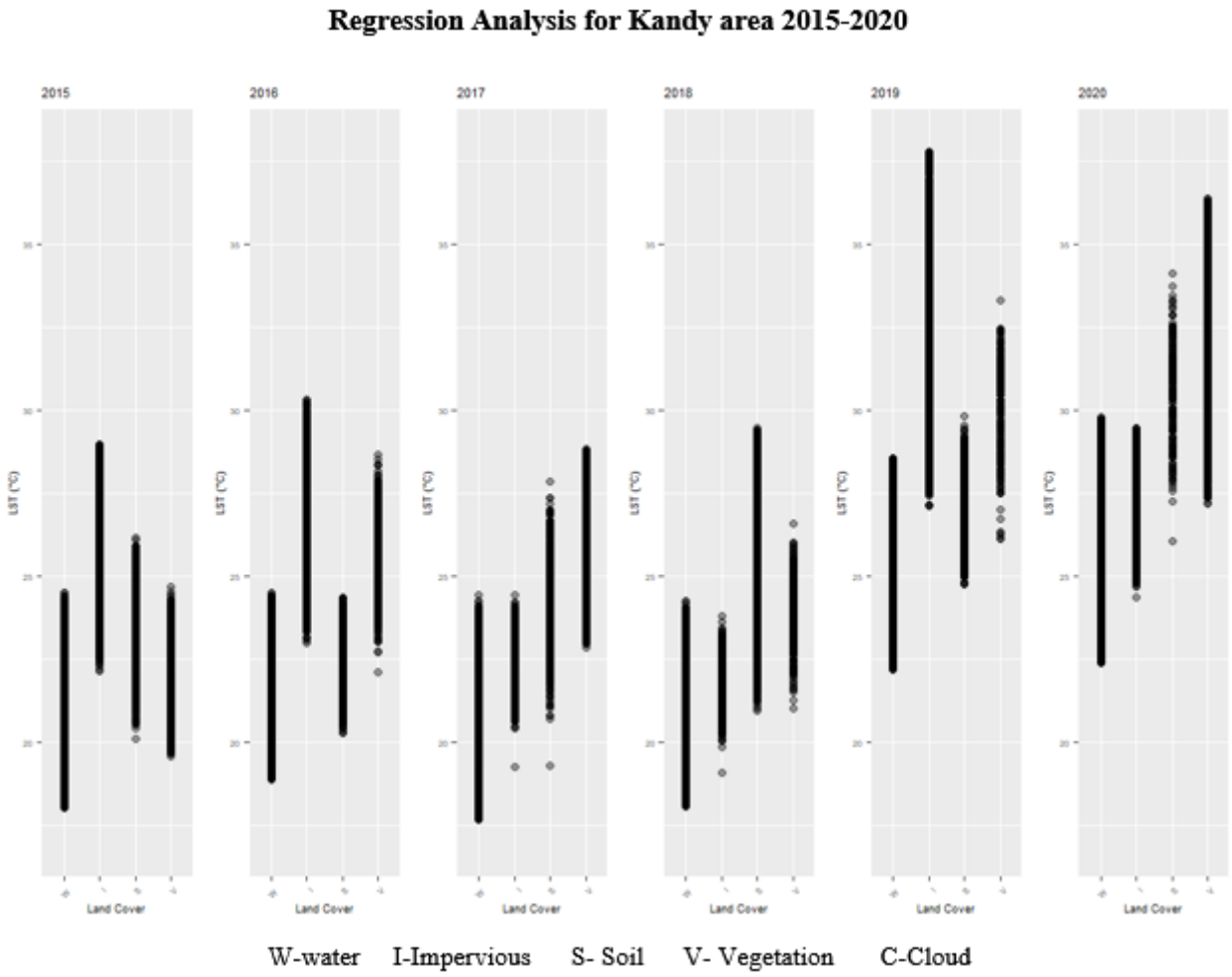

Figure 13. LST map, LC map, highly affected LCs and regression analysis of Kandy area from 2015-2020.

The Belihuloya area has a tropical rainforest climate and is at an elevation of 616 m above the mean sea level. The study area contains a part of the Samanala Wewa reservoir, where the third largest hydropower plant in Sri Lanka was commissioned. Finding cloud-free images for each year was a quite challenging task, and we had to select the images with the minimum amount of cloud cover (less than 10% for the area). According to the LC classification maps, 70% of the area is covered by vegetation and 20% by impervious surfaces. The lowest average LST over the selected main cities was recorded in the Belihuloya area with 21 C. The highest LST and the lowest LST were recorded at 19.780 C in 2017 and 23.880 C in 2019, respectively. According to the model, the highest LST values were obtained due to the soil and impervious LCs, the middle LST values were caused by the water surface, and the lowest LST values were caused by the clouds and vegetation covers. Regression analyses have also proved that the highly affected LCs for the LST changes are similar to the LCs obtained by the model.

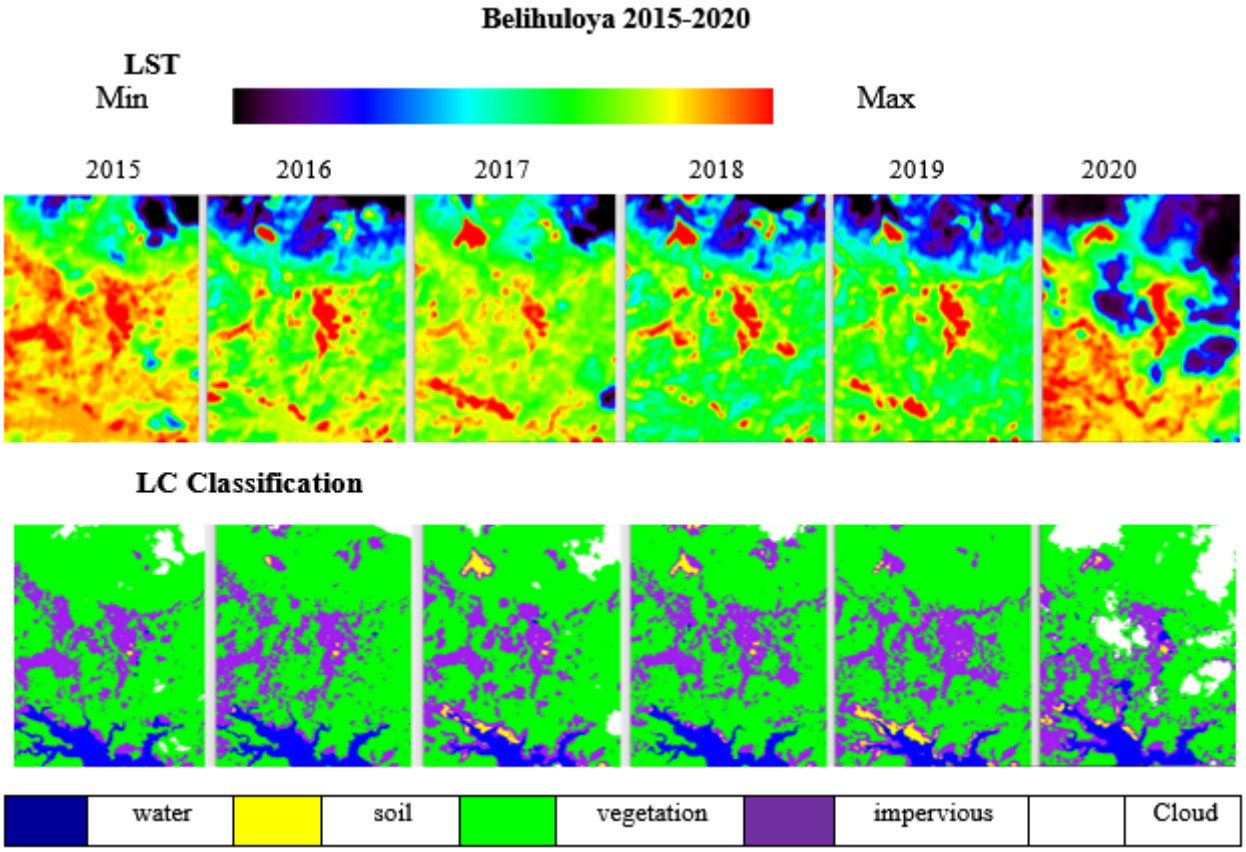

Highly effected LC classes for each LST range for Belihuloya area from 2015 to 2020

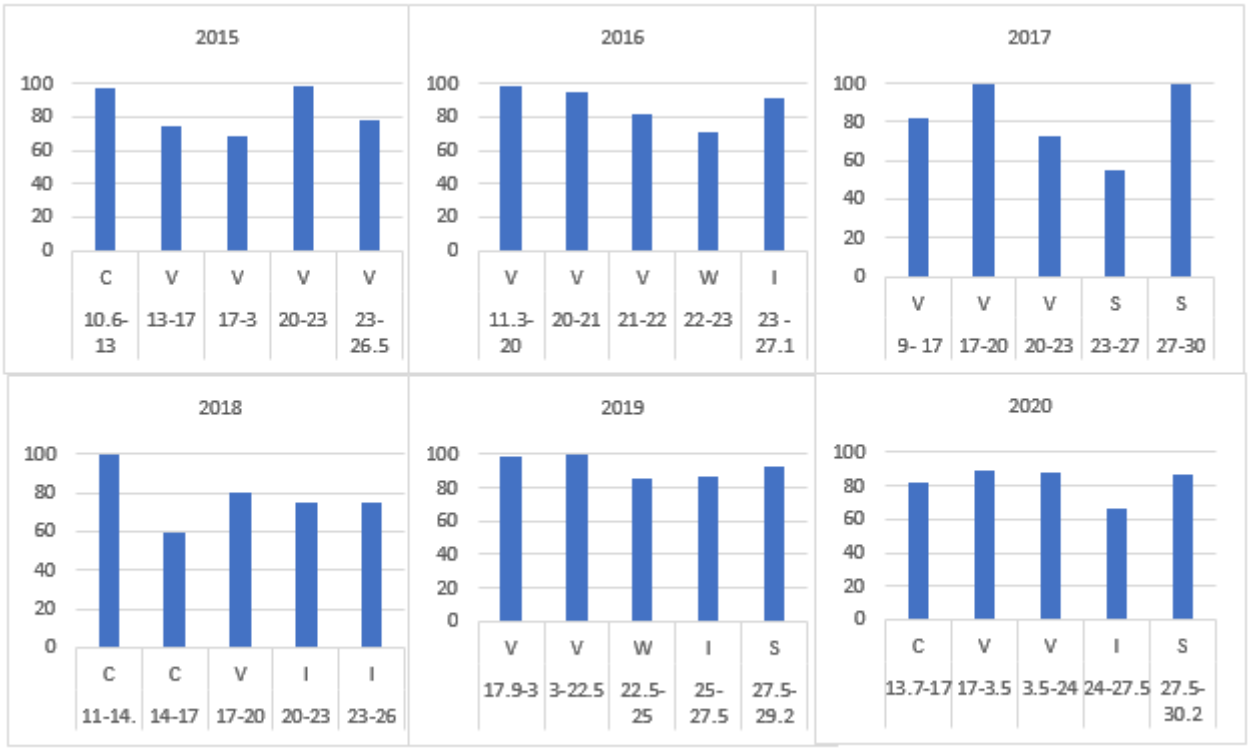

W-water I-Impervious V- Vegetation C- Cloud S-Soil
X – axis -Temperature(^{0}C) Y - axis- Percentage

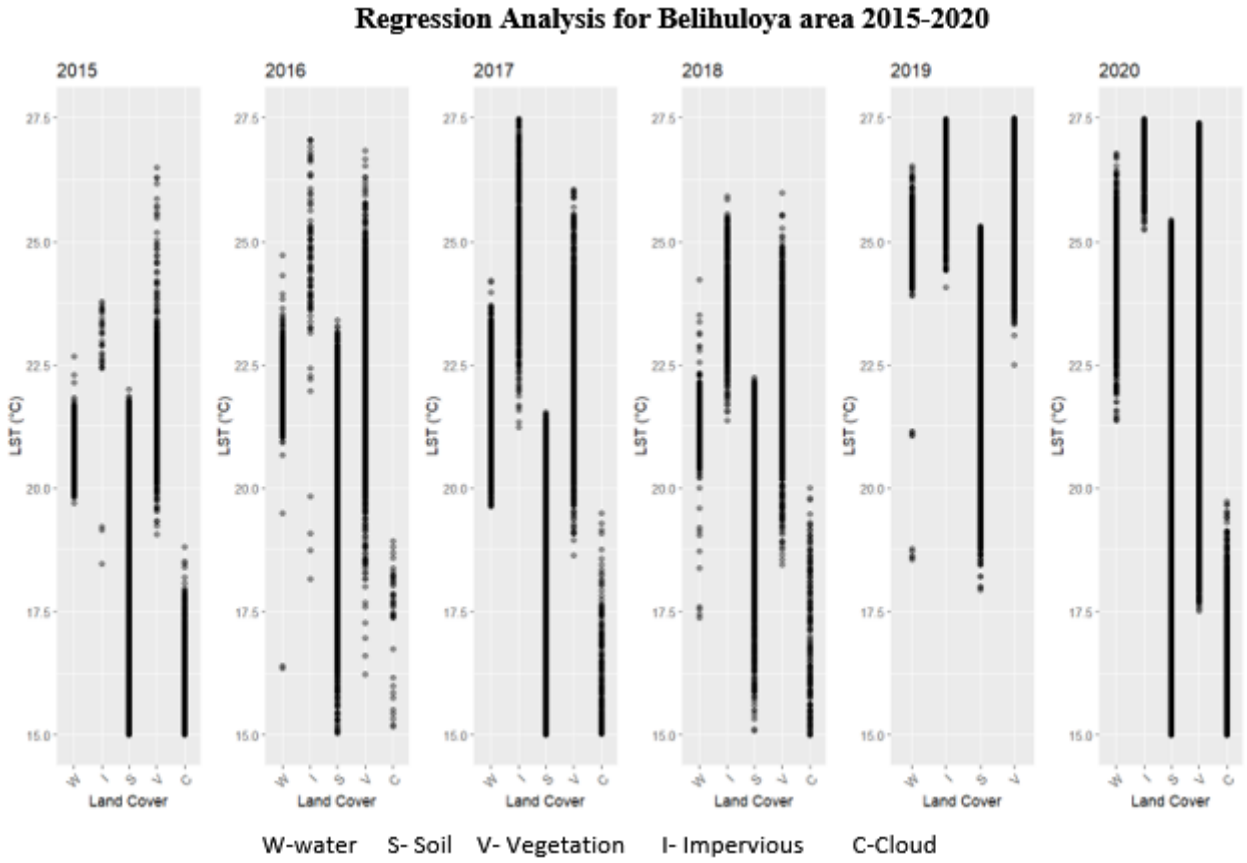

Figure 14. LST map, LC map, highly affected LCs and regression analysis of Belihuloya area from 2015-2020.

Jaffna features a tropical savanna climate, which is recorded as the highest temperature area in Sri Lanka. The selected area for the study is very close to the sea surface and has a flat terrain with around 10 m above the MSL. Both the Bayesian model and the regression analysis have shown that the highest LST has occurred due to the impervious surface in each year, but in 2016, the soil LC has been highly affected by the highest LST. The vegetation cover in 2015 was 38.9%, and in 2020 it was 33.9%. The impervious surface has increased from 47.6% to 57.9% in 2015 and 2020, respectively. The increment of the impervious surface while decreasing the vegetation surface have highly affected the LST change through the years. The highest LST has been recorded in 2018 at 28.01 C and the minimum LST was 23.81 C in 2017. The huge variation between these two consecutive years can be attributed to the misclassification of the 2018 image, which shows a waterbody inside the land area that does not really exist there, and the unexpected vegetation cover increment.

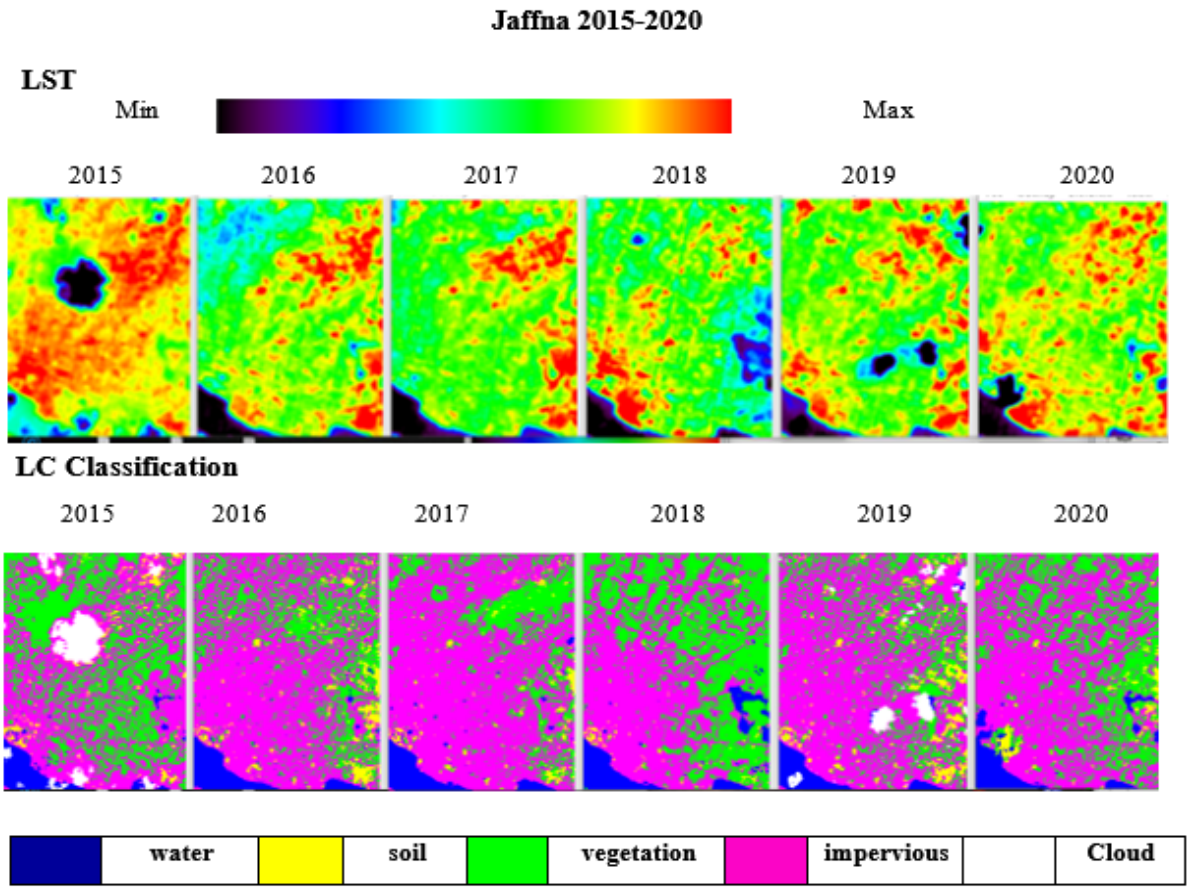

Highly effected LC classes for each LST range for Jaffna area from 2015 to 2020

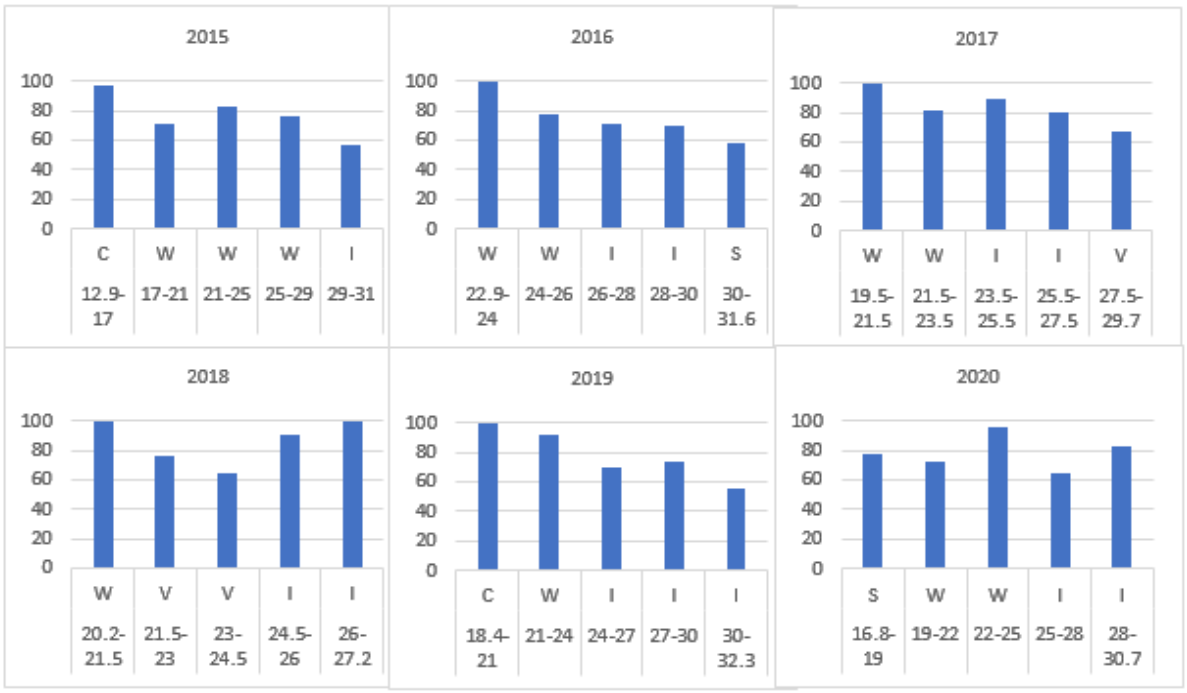

W-water I-Impervious V- Vegetation C- Cloud S-Soil
X Axis-Temperature(^{0}C) Y axis- Percentage

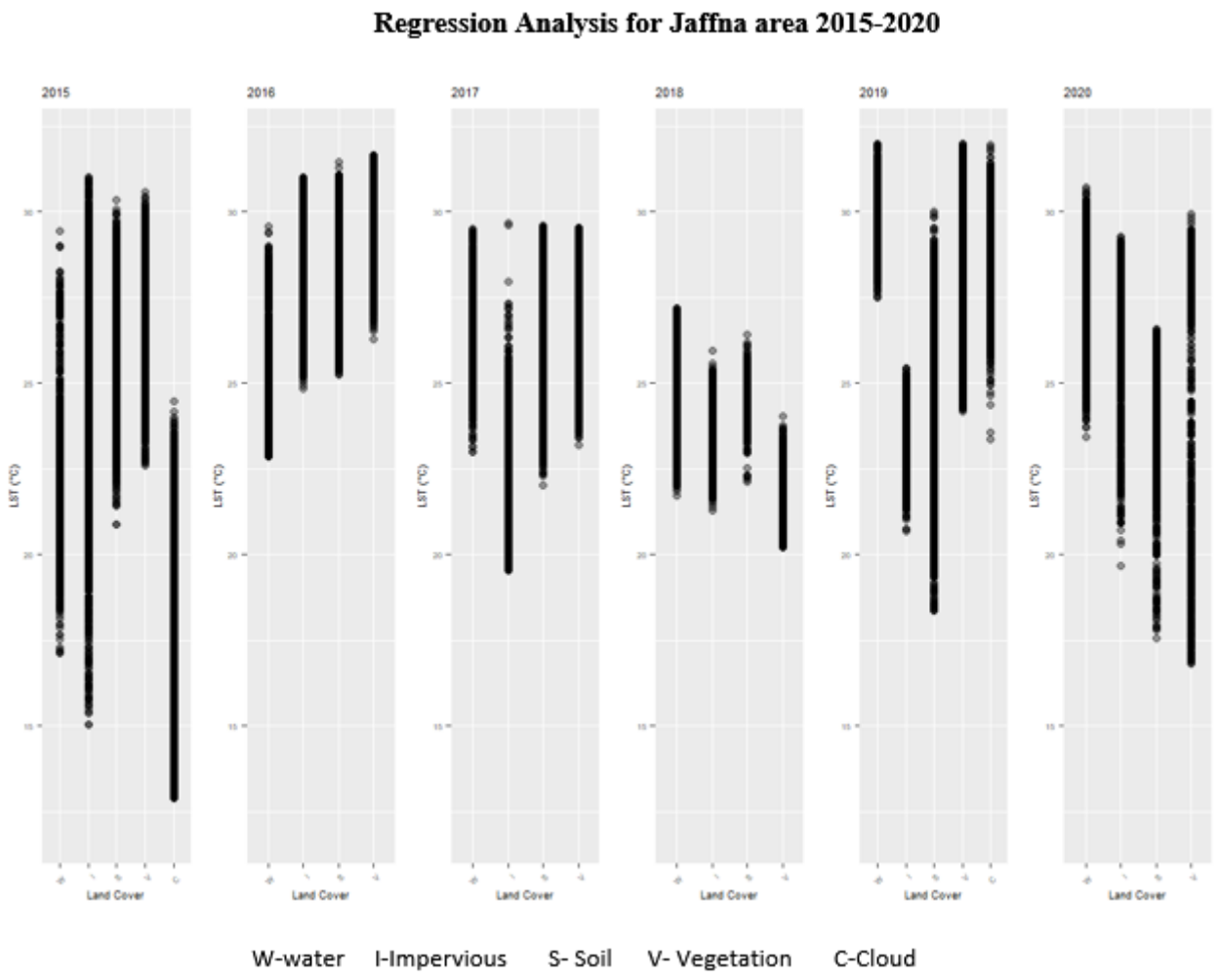

Figure 15. LST map, LC map, highly affected LCs and regression analysis of Jaffna area from 2015-2020.

The LC classification map shows that around 92% of the area is covered with vegetation and 4% is covered with water (Figure 16). The impervious and soil surface had the greatest influence on the LST, according to the e model, while the cloud and vegetation cover had the greatest influence on the lowest LST values. The average LST for the three years 2015, 2017 and 2020 has been recorded at 23.25718 C. The highest and lowest LSTs were obtained in 2017 and 2015, respectively.

Sinharaja is a forest reserve and a biodiversity hotspot in Sri Lanka that has been designated a Biosphere Reserve and World Heritage Site by UNESCO. The average LST was recorded at 21.36 C, where the vegetation cover is around 79% and the water cover is around 7% over the area (Figure 17). The model has shown that the highest LST values are mostly affected by the impervious LC, while vegetation and cloud cover affect the lowest LST values. Regression analysis shows that the middle LST values are caused by the soil and water surfaces, while the impervious surface is highly affected by the highest LST values.

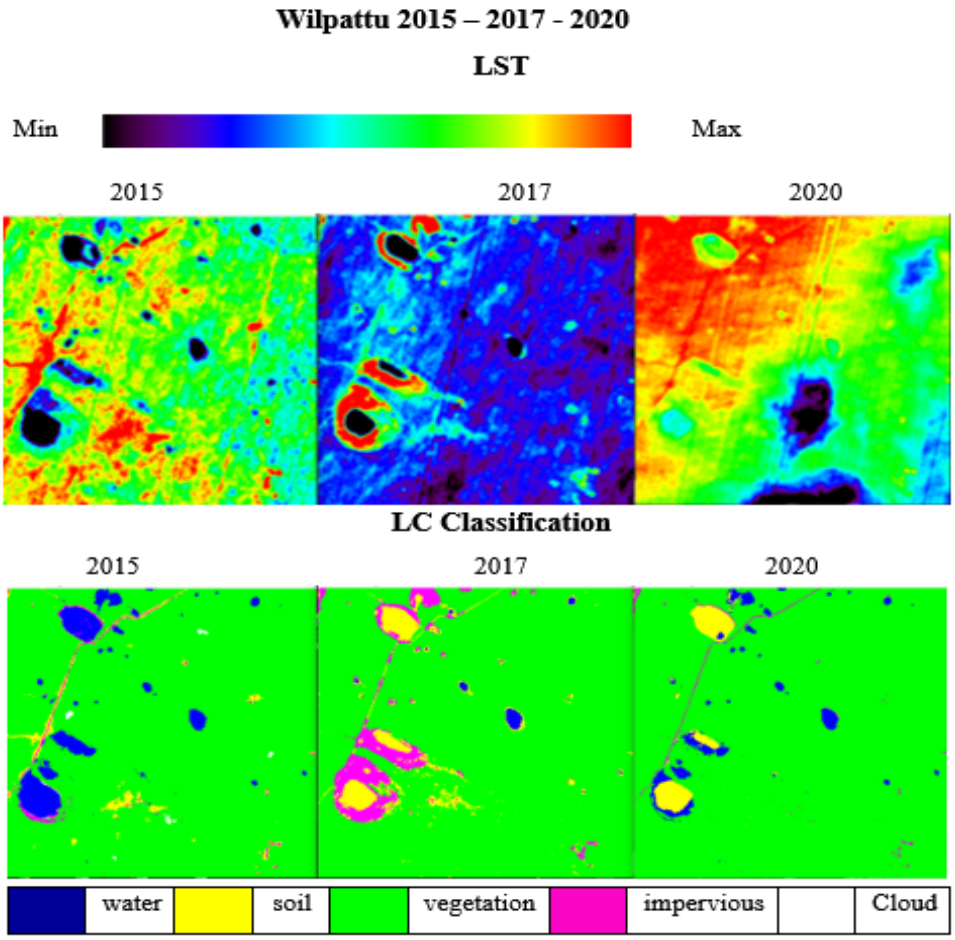

Highly effected LC classes for each LST range for Wilpattu area

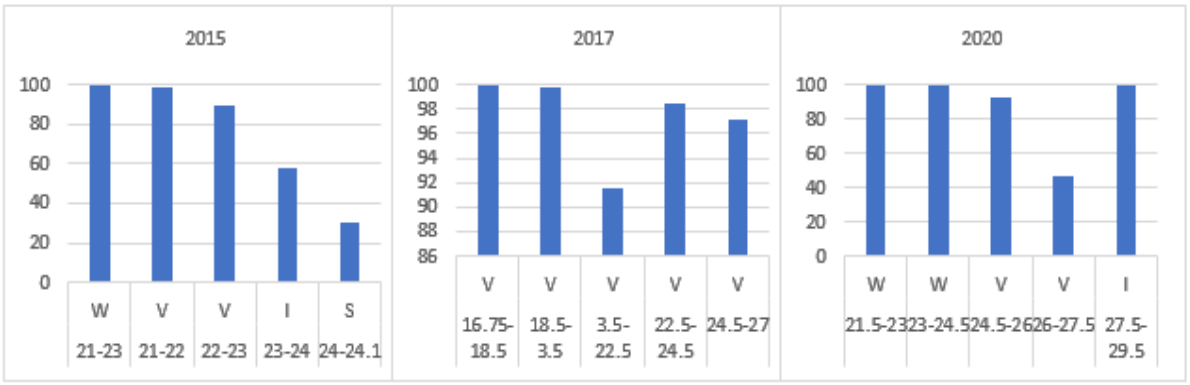

W-water I-Impervious V- Vegetation C- Cloud S-Soil
X Axis-Temperature(^{0}C) Y axis- Percentage

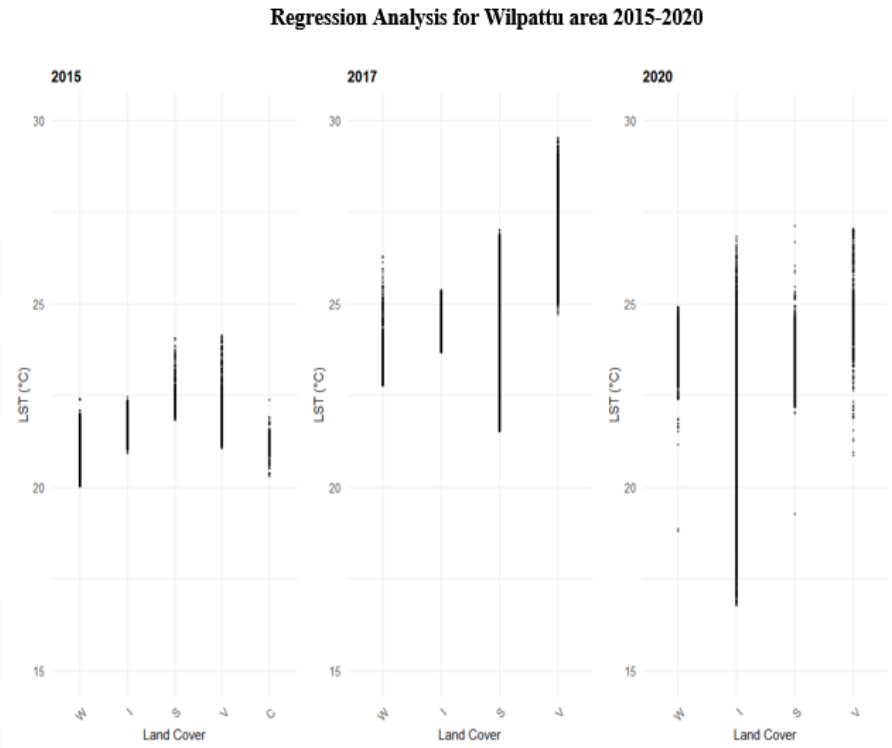

Figure 16. LST map, LC map, highly affected LCs and regression analysis of Wilpattu area from 2015-2020.

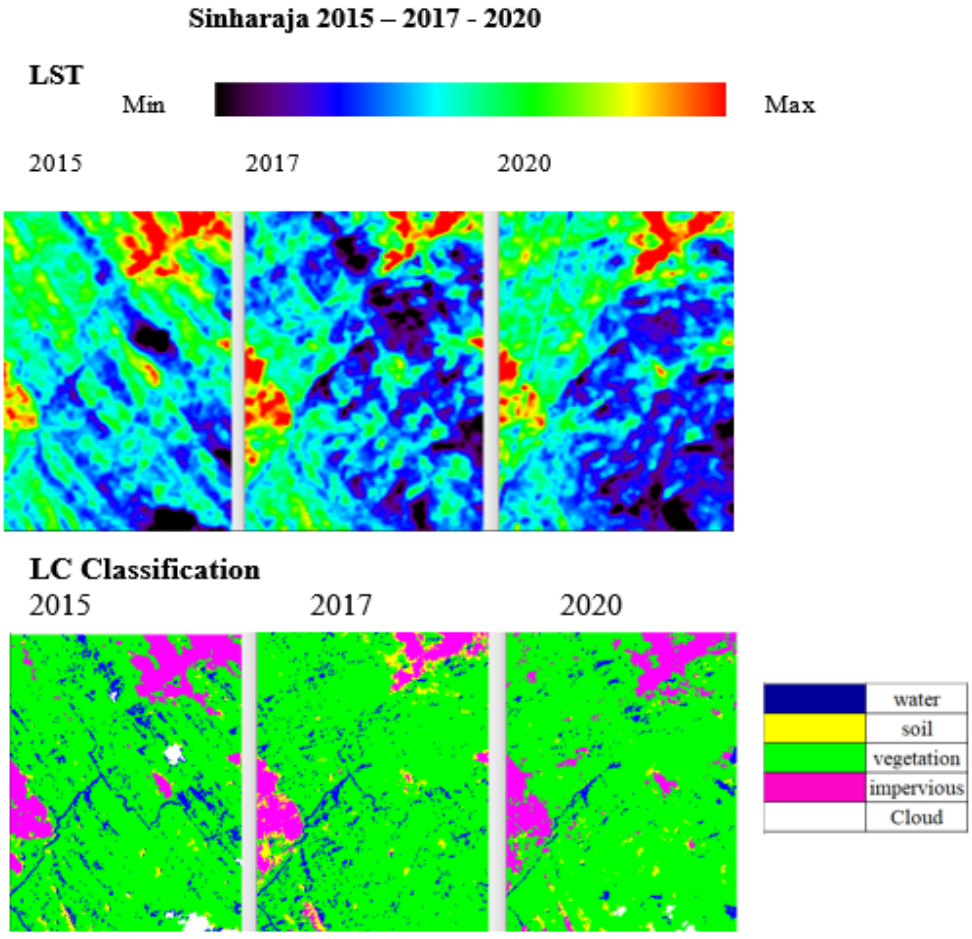

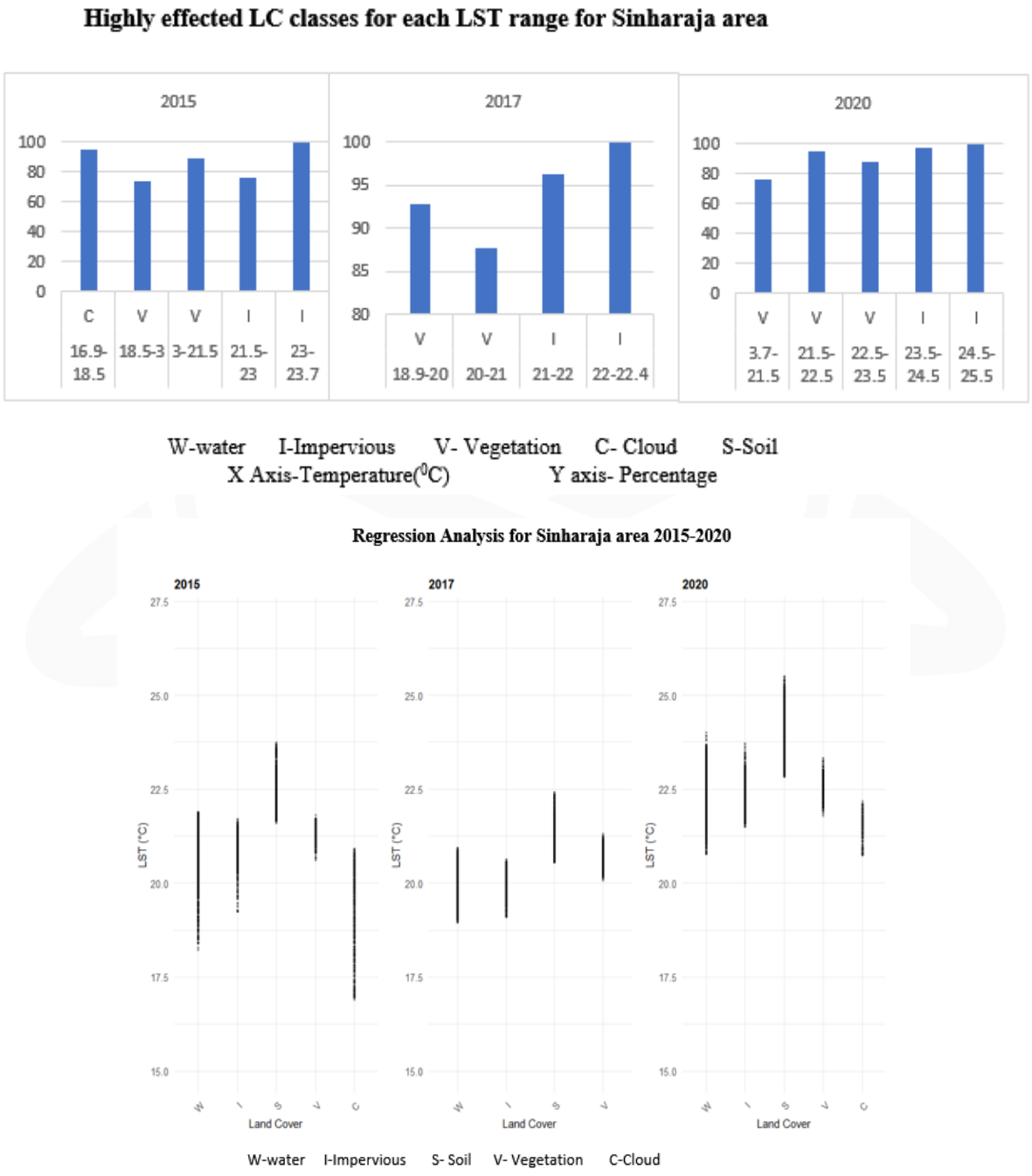

Figure 17. LST map, LC map, highly affected LCs and regression analysis of Sinharaja area from 2015-2020.

The LC maps have shown the vegetation cover at around 68%, soil at 21%, water at 4%, and impervious at 4% over the area (Figure 18). The lowest LST has been recorded in Horton Plains when compared with the other areas in the study, which are 17.93 0C on average. Soil and impervious surfaces have been highly affected for the highest LST values, and vegetation and cloud covers are affected for the lowest LST values. The middle LST values have been affected by water, but not the highly affected LC for those values. Regression analysis also shows that the highest of the LST values are affected by the soil and impervious surface.

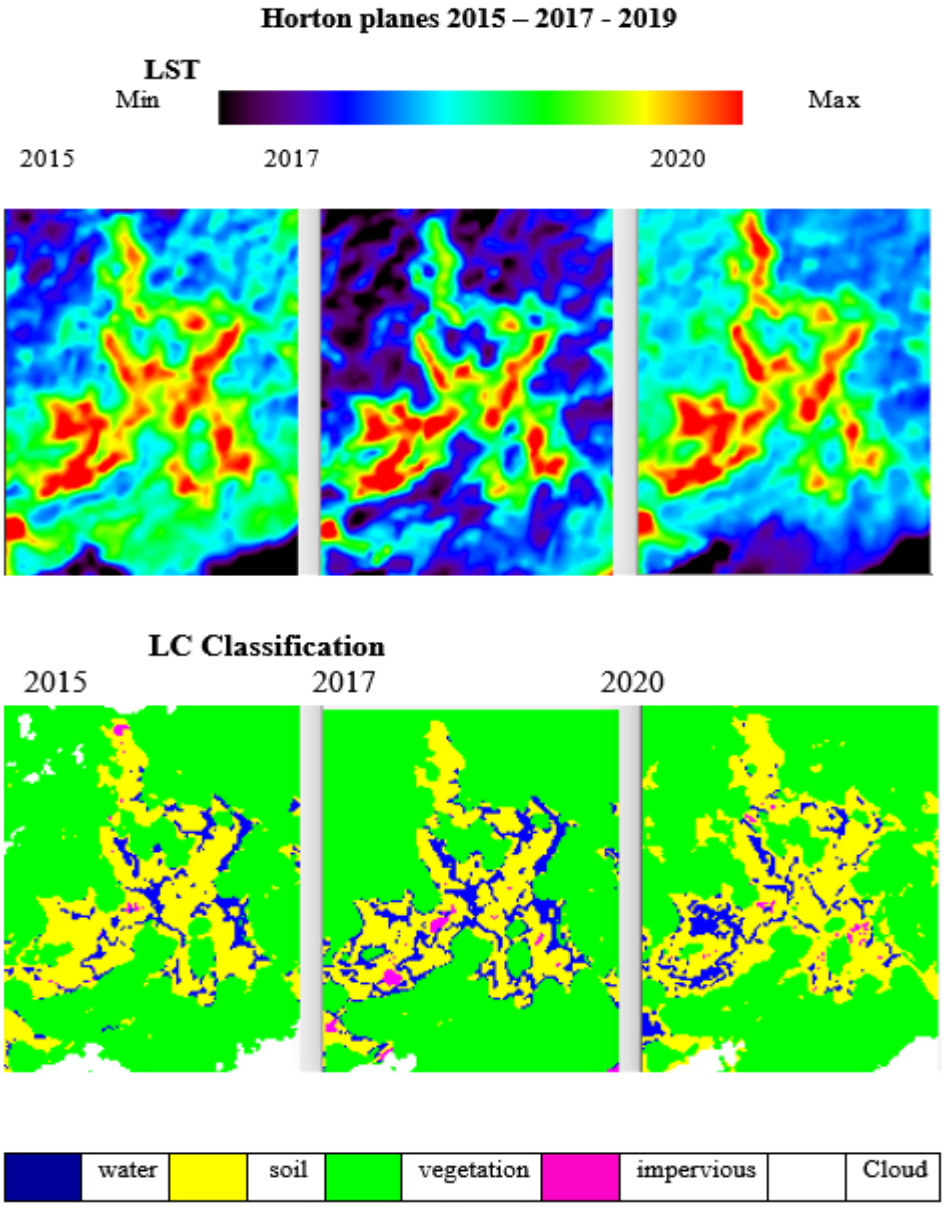

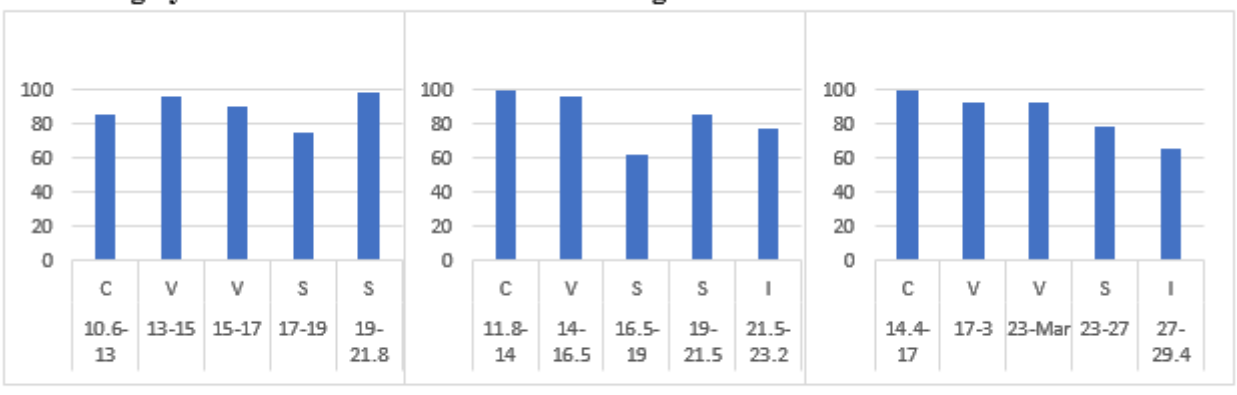

W-water I-Impervious V- Vegetation C- Cloud S-Soil

X Axis-Temperature(^{0}C) Y axis- Percentage

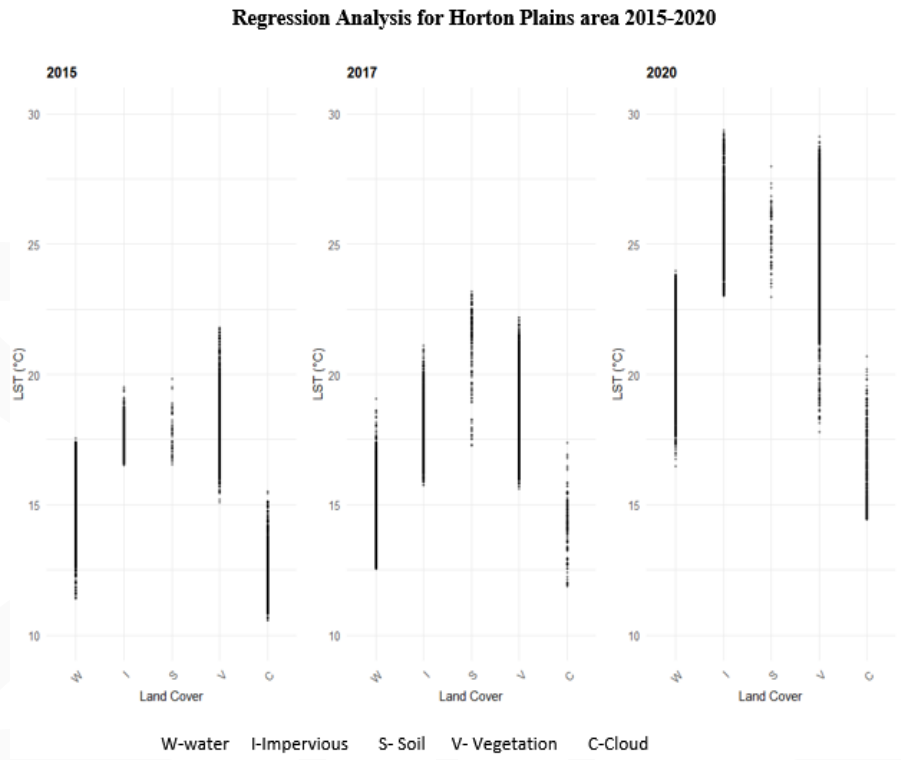

Figure 18. LST map, LC map, highly affected LCs and regression analysis of Horton Plains area from 2015-2020.

DISCUSSION

Incorporating the three parameters LST and LULC into a single Bayesian framework for estimate and prediction was the main goal of this study. The model was built using two sample datasets (8x8 matrix) for LST and LC while taking into consideration a 3x3 moving window. It was based on the Bayes theorem. Finally, model validation was carried out for a well-known area where LC changes happened in two consecutive years as a result of a huge landslide and the area's vegetation cover changing into soil. The association between LST and LC changes for each chosen research area was then investigated using the model using a time series analysis, and the most affected LCs for each temperature class were discovered. There, the LC classification and all of the LST values for each area were determined. The average LST for each region (main cities) in each year is shown in the table below. Ultimately, an average LST for six years was determined. There all the LST values for each area was calculated and LC classification was performed.

The present study developed and applied a Bayesian framework to integrate Land Surface Temperature (LST) and Land Use/Land Cover (LULC) information for estimating and predicting spatial temperature variations. The proposed model successfully incorporated both parameters into a unified probabilistic structure, enabling a more comprehensive understanding of the dynamic relationship

between surface temperature and land cover transitions. Model validation conducted in an area affected by a major landslide further demonstrated the framework's capability to identify temperature changes corresponding to vegetation loss and conversion to bare soil, highlighting the strong dependency of LST on LULC variations.

Following table is showing the average LST for each area (major cities) in each year and finally average LST was calculated for 6 years.

Table 2. Average LST for major cities (Colombo, Kandy, Belihuloya, Ratnapura and Jaffna) from 2015 to 2020.

Area	2015	2016	2017	2018	2019	2020	Average
Kandy	22.4276	23.5284	22.7608	22.6021	28.1680	28.5294	24.6694
Colombo	24.0286	26.2861	24.6971	25.1572	25.5283	27.4104	25.5179
Belihuloya	19.8269	21.0165	19.7809	20.8733	23.8845	20.6441	21.0044
Ratnapura	22.9479	23.9633	23.0841	23.4869	26.0189	25.7265	24.2046
Jaffna	25.6564	27.8384	25.8820	23.8142	28.0135	26.9540	26.3597

Among the major cities in Sri Lanka that were chosen, Belihuloya has the lowest average LST and Jaffna has the highest average LST, with a mean LST of 26.36 0C throughout the years from 2015 to 2020. This pattern aligns with the climatic and land cover characteristics of these regions. Jaffna, located in the dry zone with limited vegetation and higher impervious surface proportions, tends to accumulate more heat, whereas Belihuloya, situated in a highland environment with dense vegetation and greater elevation, promotes cooling through evapotranspiration and canopy shading. These results are consistent with findings by Weng et al. (2004) and Guha et al. (2020), who reported that vegetation cover substantially mitigates LST by enhancing latent heat flux and surface moisture availability.

The temporal analysis further demonstrated a gradual increase in mean LST values from 2015 to 2020 in most cities, suggesting possible urbanization and reduction in vegetation density. This observation aligns with Fu and Weng (2015) and Tan et al. (2020), who highlighted that urban expansion and impervious surface growth significantly contribute to the intensification of surface temperatures and the urban heat island effect. The lowest LST ranges are induced by cloud and vegetation cover when taking into account the heavily affected LC classes for each LST range, whereas water class has a significant impact on the intermediate LST values. Highest LST Values are caused due to the impervious and Soil classes.

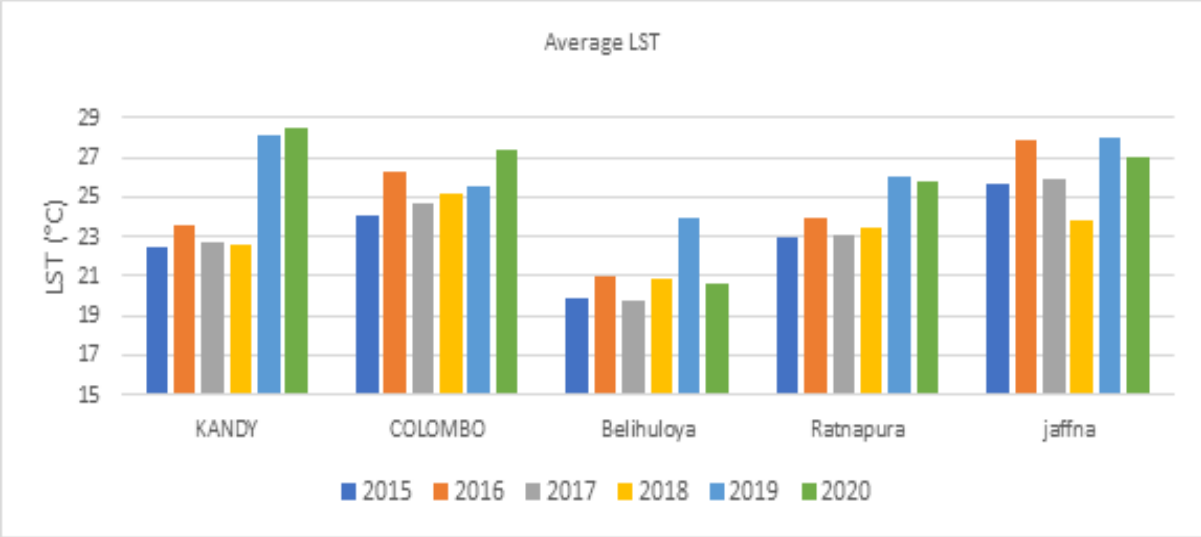

Figure 19. Average LST Graph for major cities (Colombo, Kandy, Belihuloya, Ratnapura and Jaffna) from 2015 to 2020.

Three national parks have been taken into consideration for the study to evaluate how the relationship between LST and LULC when the LCs are substantially vegetated, in addition to the major cities chosen for the study area. The Horton Plains, considered Sri Lanka's most significant watershed, a montane grassland ecosystem, exhibited the lowest average LST (17.93 °C), attributable to its high elevation, extensive vegetation, and minimal anthropogenic influence. The forest canopy rises to a height of 20 meters, and Horton Plain has the lowest impervious LC and the greatest soil LC of the other two forest sections.

potentially due to its mixed vegetation structure and seasonal dry conditions. These findings reinforce the conclusions of Sun et al. (2011) and Purevdorj et al. (2010), who emphasized that denser vegetation cover and soil moisture availability are key determinants of lower LST in forested landscapes.

Regression analyses confirmed a statistically significant relationship between LST and LC variations, particularly highlighting that the soil and impervious classes are dominant contributors to elevated LST values, while vegetation and cloud classes are associated with lower LST. The water class was found to moderate temperature, aligning with intermediate LST ranges. This classification-dependent temperature gradient supports the theoretical understanding of surface emissivity and albedo differences as described by Qin et al. (2001) and Sobrino et al. (2004). The model thus provides a practical basis for quantifying how land conversion processes, such as deforestation or urbanization, modify thermal conditions over time.

Table 3. Average LST for Wilpattu, Sinharaja and hortan planes forest areas in 2015,2017 and 2020.

Area	2015	2017	2020	Average
Wilpattu	21.7801	24.5391	23.4523	23.2572
Sinharaja	21.1882	20.2056	22.6790	21.3576
Hortan Planes	15.8388	15.8044	22.1362	17.9264

The model's outcome probability for each area demonstrates that LST is significantly impacted by LC changes, and that as vegetation cover shifts to other LCs such soil and impervious, LST increases with time. Each location underwent regression analysis to look into the relationship between LST and LC variations. It reveals how soil and impervious classes have a significant impact on the highest LST in forest areas while vegetation and cloud cover have an impact on the lowest LST. The middle LST values are affected by the water class.

While the Bayesian approach demonstrated robustness and interpretability, certain limitations should be acknowledged. The model's reliance on two sample datasets (8 x 8 matrices) and a fixed 3 x 3 moving window may have restricted spatial generalization. Moreover, the LST retrieval accuracy depends on atmospheric correction and emissivity estimation methods (e.g., Barsi et al., 2014; Avdan & Jovanovska, 2016), which could introduce uncertainty in highly heterogeneous surfaces. Future research could extend this framework using finer-resolution data, multi-seasonal imagery, and additional parameters such as NDVI, albedo, and soil moisture to improve prediction accuracy and applicability in complex urban–rural landscapes.

Overall, the findings emphasize that LULC change plays a decisive role in controlling spatial and temporal variations of LST. The integration of both parameters within a Bayesian framework provides a statistically consistent and spatially flexible method for monitoring environmental change. This approach can be applied to assess the thermal impacts of land transformation, aiding in sustainable land management, urban planning, and climate adaptation strategies across Sri Lanka and similar tropical regions.

CONCLUSION

The model can be used to find the conditional probability of each LC class with respect to the LST for each year. The model built in the study could be used to analyze relationships between parameters depending on their frequency distributions.

When comparing the regression analysis with this model, the regression analysis gives the best fitting value considering all the available data without considering the precision of the values from which it calculates the best estimate. Sometimes, there may be outliers. But this model is calculating the exact

conditional probability of each single event within the 3x3 moving window, and it is not affected by all the values in the dataset. The final output is taken with the most probable values, and if there were some outliers within the window, they will be neglected at the final output.

This model was developed only considering the effect of LC changes on LST changes. The LST changes can be affected by some other factors, such as surface soil moisture, urban heat island effect, wind speed, rainfall, and elevation. So, the model should be developed to include the other affecting parameters as well.

The study can be performed by excluding all the cloud cover effects, which have shown a highly negative relationship with LST with techniques such as the CF mask algorithm, the fog stability index, etc.

The image acquisition date may be subjected to LST variations in the trend analysis due to the dry and wet seasons, which can be highly affected by the vegetation cover and water bodies.

REFERENCES

Avdan, U., & Jovanovska, G. (2016). Algorithm for automated mapping of land surface temperature using LANDSAT 8 satellite data. Journal of Sensors, 2016, Article 1480307. https://doi.org/10.1155/2016/1480307

Barsi, J. A., Schott, J. R., Hook, S. J., Raqueno, N. G., Markham, B. L., & Radocinski, R. G. (2014). Landsat-8 thermal infrared sensor (TIRS) vicarious radiometric calibration. Remote Sensing, 6(11), 11607–11626. https://doi.org/10.3390/rs61111607

Das, S. S., & Angadi, D. P. (2021). Assessment of land surface temperature differential and its relationship with urban land use land cover change in Barrackpore Subdivision, West Bengal, India. Remote Sensing Applications: Society and Environment, 24, Article 100647. https://doi.org/10.1016/j.rsase.2021.100647

Fu, P., & Weng, Q. (2015). A time series analysis of urbanization induced land use and LC change and its impact on land surface temperature with Landsat imagery. Remote Sensing, 7(12), 16671–16698. https://doi.org/10.3390/rs71215844

Guha, S., Govil, H., Gill, N., & Dey, A. (2020). Analytical study on the relationship between land surface temperature and land use/land cover indices. Annals of GIS, 26(2), 201–216. https://doi.org/10.1080/19475683.2020.1754291

Markham, B. L., & Barker, J. L. (1985). Spectral characterization of the Landsat Thematic Mapper sensors. International Journal of Remote Sensing, 6(5), 697–716. https://doi.org/10.1080/01431168508948492

Purevdorj, T. S., Tateishi, R., Ishiyama, T., & Honda, Y. (1998). Relationships between percent vegetation cover and vegetation indices. International Journal of Remote Sensing, 19(18), 3519–3535. https://doi.org/10.1080/014311698213795

Qin, Z., Zhang, M., Karnieli, A., & Berliner, P. (2001). Estimation of land surface emissivity for Landsat TM6 data. Remote Sensing of Environment, 76(2), 229–239. https://doi.org/10.1016/S0034-4257(00)00183-1

Rhee, J., Park, S., & Lu, Z. (2014). Relationship between land cover patterns and surface temperature in urban areas. GIScience & Remote Sensing, 51(5), 521–536. https://doi.org/10.1080/15481603.2014.964455

Richards, J. A., & Jia, X. (2005). Remote sensing digital image analysis. Springer-Verlag.

Sobrino, J. A., Jimenez-Munoz, J. C., & Paolini, L. (2004). Land surface emissivity retrieval from different VNIR and TIR sensors. IEEE Transactions on Geoscience and Remote Sensing, 42(2), 316–321. https://doi.org/10.1109/TGRS.2003.821064

Sun, Q., Wu, Z., & Tan, J. (2012). The relationship between land surface temperature and land use/land cover in Guangzhou, China. Environmental Earth Sciences, 65(6), 1687–1694. https://doi.org/10.1007/s12665-011-1145-2

Tan, J., Yu, D., Li, Q., Tan, X., & Zhou, W. (2020). Spatial relationship between land-use/land-cover change and land surface temperature in the Dongting Lake area, China. Scientific Reports, 10(1), Article 9245. https://doi.org/10.1038/s41598-020-66168-6

Weng, Q., Lu, D., & Schubring, J. (2004). Estimation of land surface temperature–vegetation abundance relationship for urban heat island studies. Remote Sensing of Environment, 89(4), 467–483. https://doi.org/10.1016/j.rse.2003.11.005

Xu, H. Q., & Chen, B. Q. (2004). Remote sensing of the urban heat island and its changes in Xiamen City of SE China. Journal of Environmental Sciences, 16(2), 276–281.